I&EC research
Industrial & Engineering Chemistry Research
pubs.acs.org/IECR
Article

Comprehensive Modeling and Optimization of Standby Mechanisms in Continuous Chemical Plants

Cheng-I Tu and Chuei-Tin Chang*

Cite This: *Ind. Eng. Chem. Res.* 2023, 62, 5150−5169
Read Online
ACCESS | Metrics & More | Article Recommendations | Supporting Information

ABSTRACT: In a continuously operated chemical plant, not only the critical unit may fail after a long period of operation, but also its process load may vary from time to time. Thus, it is necessary to incorporate standby mechanisms to maintain uninterrupted production and also satisfy the unexpected increases/decreases in external demands throughout the operation horizon. Although a few related studies were reported in the literature, a comprehensive analysis of multilayer standby mechanisms in continuous processes still has not been carried out. To address this need, a generalized mathematical programming model has been constructed in this work to automatically synthesize the optimal designs and maintenance policies of the standbys for any continuous process by minimizing the total expected lifecycle expenditure. A MATLAB code has been developed to execute the optimization runs via genetic algorithm. The feasibility and effectiveness of the proposed model and solution method are demonstrated in this paper with case studies concerning the pump systems in a typical chemical plant. From the optimization results, one can obtain proper design specifications of the standby mechanisms, which include: (1) the number of protection layers (or online warm standbys) and the number of cold standbys stored offline; (2) the numbers of installed sensors in each measurement channel, the corresponding voting-gate logic, and their spares; and (3) the inspection interval of switch and the number of its spares.

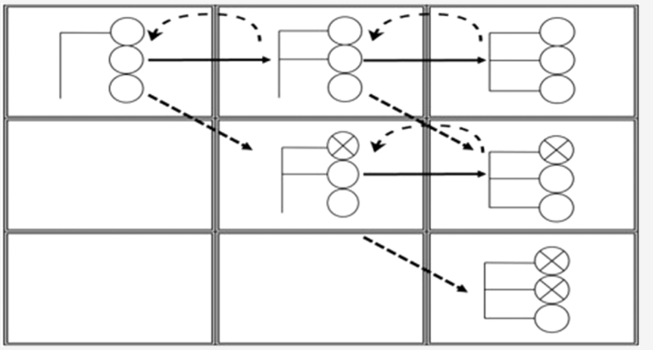

1. INTRODUCTION

The design of a critical unit in a process plant usually incorporates standby mechanism to improve its reliability, that is, to maintain uninterrupted production and also to withstand the varying load throughout the operation horizon. According to Zhang et al.,[1] there are three types of standbys. The "hot standbys" refer to a collection of identical components arranged in parallel and all are loaded equally online. On the other hand, the "warm standby" means such this unit also works online but under a much lighter load and, thus, its failure rate is considerably lower than its hot counterpart. If an online unit is broken, then the warm standby is supposed to take its place right away. Finally, the "cold standby" is usually stored offline in the warehouse and its failure rate is almost zero. A full-fledged standby should consist of the monitors, the switch, and the remedial device(s).

If the above mechanism is configured manually according to experience, it is obviously difficult to obtain an optimal design due to the complex nature of the system structure. Although Chan et al.[2] have already developed a mathematical programming model for designing the multilayer standby mechanisms under a constant load and Chan and Chang[3] developed another model to automatically synthesize the optimal designs and maintenance policies of the standby mechanisms in short-term operations under varying loads, a complete analysis of both the reliability of critical units and also the downstream demands still has not been attempted. Therefore, there are strong incentives to construct a comprehensive model to determine the optimal standby system configuration and its maintenance policy in a wide variety of industrial environments.

Each hardware item in a standby system may fail either safely (FS) or dangerously (FD), while a failure may be either revealed or hidden. It is assumed in this study that the FS and FD sensor failures are observable and, therefore, the upkeep of monitoring subsystem can be facilitated with corrective maintenance policy. Kuo and Zuo[4] suggested using multiple redundant sensors to monitor the same process variable and then applying the voting gate to determine if this variable is within the normal range. Liang and Chang[5] proposed a spare-supported corrective maintenance policy for improving the reliability of monitoring subsystem. Liao and Chang[6] extended this practice to multichannel monitoring strategy. The alarm and/or protective

Received: December 16, 2022
Revised: March 6, 2023
Accepted: March 7, 2023
Published: March 16, 2023

https://doi.org/10.1021/acs.iecr.2c04521
Ind. Eng. Chem. Res. 2023, 62, 5150−5169

measure were triggered via an online logic based on measurements of different process variables. It is believed that this approach can further enhance the system reliability.

The hidden failures of switch and warm standby(s) can only be detected on demand and, if otherwise, their symptoms are not observable online. Preventive maintenance policies, that is, inspecting the above components periodically and repairing them or replacing them with good ones when necessary should be adopted to suppress the chances of hidden failures. Vaurio[7] introduced the age-based replacement strategy into the preventive maintenance policy and proposed to determine the inspection interval by minimizing cost. After a fixed number of inspections and maybe subsequent repairs, the inspected component must be replaced with a new one even if it is still functional. Badía et al.[8] assumed that only hidden failures took place in a given system and also assumed that inspections were imperfect. They estimated the length of inspection interval again by minimizing cost. Under the assumptions that the failure rate increases linearly with time and the repair rate is constant, Duarte et al.[9] synthesized the cost-optimal preventive maintenance policy.

On the other hand, numerous studies have also been carried out to analyze the standby mechanisms. By viewing a two-unit standby system as a Markov renewal process, Nakagawa and Osaki[10] constructed a mathematical model to predict the corresponding failure rate, repair rate, and time-dependent failure probabilities, and Nakagawa[11] further suggested that switch failures may be classified as permanent and temporary. Pan[12] explored the impacts of sensor failure rate and imperfect switch and warm standby on system reliability. On the basis of Markov state diagram, Raje et al.[13] carried out availability analysis for a two-pump standby system. Yun and Cha[14] studied the effects of switching time on the reliability of a two-unit warm standby system. Zhong and Jin[15] developed the optimal preventive maintenance policy for cold standby systems according to semi-Markov theory. Hellmich and Berg[16] applied Markov analysis to standby safety systems under constant-interval inspections. Levitin et al.[17] introduced random replacement times into a one-out-of-N warm standby system. Based on Markov process and nondominated sorting genetic algorithms (NSGA-II), Kayedpour et al.[18] proposed a computation strategy to determine the maximum reliability and minimum expected expenditure of any standby system. Zhu et al.[19] optimized standby system design by considering various costs. On the other hand, the multivalued decision diagram (MDD) has also been widely applied in designing standby systems, e.g., Zhai et al.,[20] Jia et al.,[21] and Naithani et al.[22] made use of semi-Markov model and regenerative point technique to evaluate the reliability of standby systems. Finally, the multivalued decision diagram (MDD) and the multistate decision diagram (MSDD) have been utilized in numerous studies, e.g., Amari et al.,[23] Jia et al.[24] and Ruan and Lin,[25] etc., for assessing the reliability of standby systems.

Since the aforementioned works are mostly limited to small-scale systems or systems with fixed configurations, it is difficult to extend these reported approaches to other applications. Chan et al.[2] assumed in their study that the given online units and their standbys were operated over a long period of time under constant process load and, thus, only the hardware reliability was under consideration. In a later study, Chan and Chang[3] considered the scenario that the operation horizon was relatively short and the process load varied frequently. As a result, the design objective was to satisfy changing demand but not the reliability of online units and standbys. Both studies mentioned above produced cost-optimal standby configurations obtained by solving mathematical programming models according to superstructures and event trees. Although satisfactory results were reported, the applicability of these proposed models was still limited by their assumptions. Running a continuous chemical process in a realistic environment is supposed to be a long-term operation and, over this time horizon, not only the online units or their standbys may experience failures but also the process load may vary from time to time. Therefore, there is a need to construct a comprehensive model to address all configurational and maintenance issues so as to generate the most appropriate standby design. Finally, it should be noted that the variations of "loads" or "shocks" in our work were assumed to follow different homogeneous Poisson processes[26] respectively and all process parameters were given a priori. On the other hand, notice that the currently popular data-driven models[27,28] were supposed to be obtained primarily on the basis of actual online measurement data. Since designing and maintaining optimal standby systems are considered in the present study, the online data of shocks (i.e., equipment failures and abnormal process demands) are really scarce and hard to come by. Therefore, the above-mentioned former modeling approach was adopted in the present work.

2. CONCEPTUAL CHARACTERIZATION OF STANDBY MECHANISM

Let us assume that, over the entire horizon of the plant operation, the critical online processing unit(s) may experience failures, load increases, and decreases and these events take place independently according to a distinct homogeneous Poisson process.[26] For example, the instrument air used to manipulate the pneumatic control valves in a chemical plant maybe supplied with a group of fans[29] and, among them, one or more unit is running and the rest are on standby. If any online unit fails, one of the warm standbys is supposed to take its place right away. On the other hand, instrument air demand may fall or rise unexpectedly, and the fan system should respond appropriately to match the downstream needs. Specifically, one or more online units must be taken offline in the former case, while a warm standby switched on to provide extra capacity in the latter. In this study, the above switching actions were assumed to be carried out either by human operator(s) or by automatic control devices (see Liptak[29]). As a second example in plant operations, the pumps transferring fluid to feed a distillation column could in principle face the same decisions in identical scenarios. Finally, it may also be possible to address similar issues in operating multiple gas turbines in a power plant with the analytic approach presented in the following.

To characterize the aforementioned operations clearly, let us consider the specific case of a four-unit standby system. To facilitate rigorous analysis, the system operations are classified into four modes according to their structures and they are, respectively, referred to as Mode I, Mode I^0, Mode II, and Mode II^0, in this paper. Every Mode-I configuration consists of only a single functional online unit and one or more warm standby, while the Mode-I^0 structure is also equipped with just one online unit but it is without any standby. Consequently, there should be at least two units running under Mode II or Mode II^0. In this study, the warm standby(s) is still available in Mode I and Mode II, but none operable in the other two modes.

Let us next place all of the above-mentioned standby structures in a conceptual 4-by-4 upper triangular matrix given

https://doi.org/10.1021/acs.iecr.2c04521
Ind. Eng. Chem. Res. 2023, 62, 5150−5169

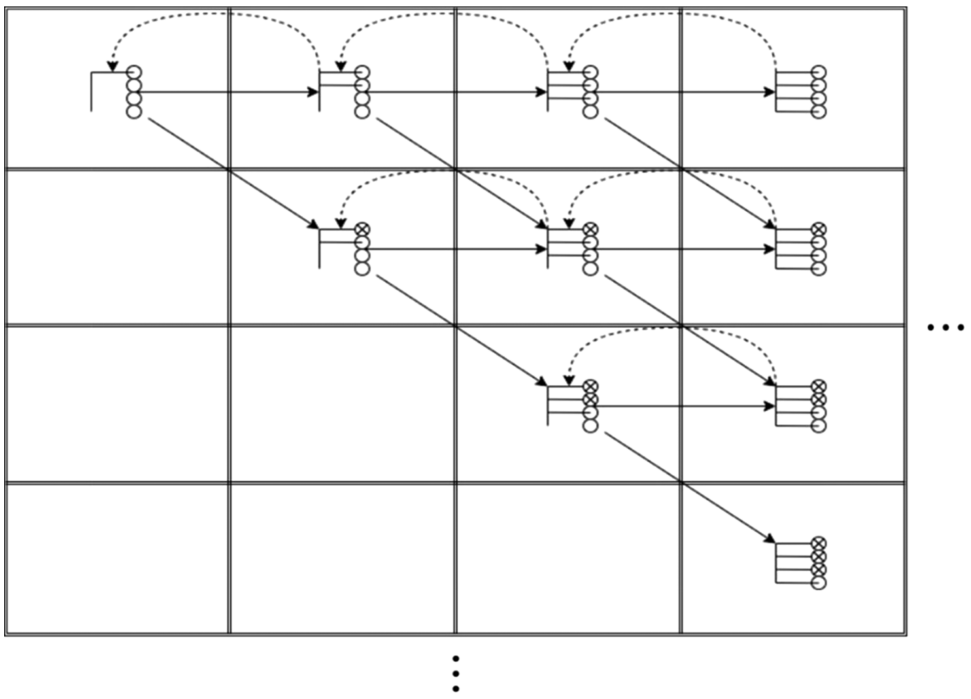

Figure 1. Structural transformation matrix used to show all structure-to-structure transition routes.

in Figure 1. Notice that the entries along and above the diagonal line in this matrix are filled with configurational symbols and one example is shown in Figure 2 for illustration purpose. All circles

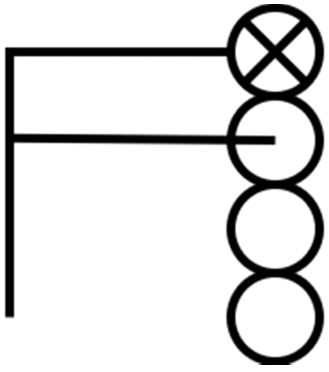

Figure 2. Example of configurational symbol of the standby system.

in this figure are used to represent a unit in the standby system. A circle connected with a horizontal solid line means the corresponding unit is running online, while every unconnected one is treated as a warm standby. Any failed online unit is marked with an "X", while the functional ones are left empty.

All possible structural transition processes in the above four-unit standby system can be expressed explicitly with the directed arcs in Figure 1. As shown in this figure, a configuration may be connected with solid arcs pointing to the right and to the lower right, respectively, and also with a dotted arc pointing to the left. These three types of transitions are resulting from the events (shocks) of load increase, online unit failure, and load decrease, respectively, under the condition that all components (other than the failed ones) function correctly. Notice also that the operating conditions associated with each entry in this matrix can be uniquely identified according to its row number (r) and column number (c). The number of damaged units should be $r - 1$, while the total number of units not taken offline (including those currently in use and also the broken ones) is c. Thus, the number of warm standbys should be $L - c$, where L is the total number of units incorporated in the given system or simply the dimension of the square matrix. For the sake of computation simplicity, every damaged processing unit is assumed to be left online without repair in this study. Finally, it is also assumed that the aforementioned three types of events do not occur at exactly the same time.

The configuration in the entry at lower-right corner of the structural transition matrix in Figure 1 should be classified as Mode I^0, while all others in the remaining entries in the last column can be referred to as Mode II^0. All diagonal entries (except the entry in which Mode I^0 is located) should be considered to be under Mode I. By excluding the entries in which Mode I^0, Mode II^0, and Mode I are located, the other configurations in the remaining entries can be designated as Mode II. Finally, let us consider the generalized case of an L-unit system. Based on the above discussion, one could deduce that there should be $L - 1$ Mode-I configurations, 1 Mode-I^0 configuration, $\frac{(L-1)(L-2)}{2}$ Mode-II configurations, and $L - 1$ Mode-II^0 configurations.

To facilitate clearer understanding of the above transition processes, more general descriptions should be made available to further characterize all hardware items embedded in the standby systems and also their interconnections. In fact, this so-called "superstructure" has already been developed and fully explained in Chan et al.[2] and Chan and Chang.[3] For the sake of brevity, this material is omitted from the main body of the present paper and placed in Part A of the Supporting Information (SI) instead.

3. EVENT TREES

As mentioned previously in the Introduction section, the objective of the present study is to develop a mathematical programming model for generating the optimal standby/

https://doi.org/10.1021/acs.iecr.2c04521
Ind. Eng. Chem. Res. 2023, 62, 5150−5169

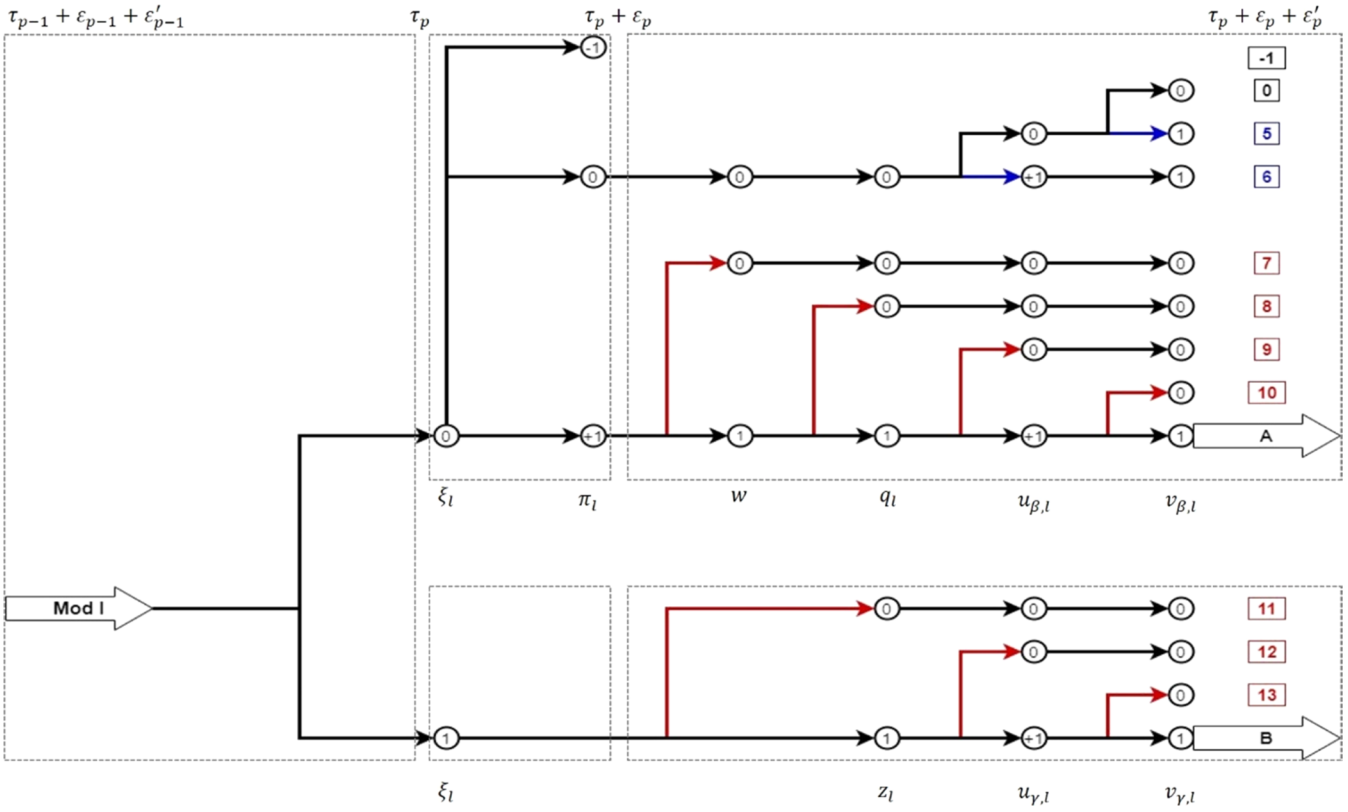

Figure 3. Event tree for Mode I.

fallback system designs and the corresponding maintenance policies. To reach this goal, a more detailed system description is needed. Let us assume that the total length of operation horizon is H and consider any time instance t in this horizon, i.e., $0 < t \leq H$. In addition, let τ_p be the time point at which the pth ($p = 1, 2, \cdots$) "shock", i.e., load increase, load decrease, or online unit failure, occurs before t. Specifically, $0 = \tau_0 < \tau_1 < \tau_2 < \cdots < t$ and it is also assumed that only one shock may happen at any given time point. The standby configuration is assumed to be unchanged in the interval $[\tau_{p-1} + \varepsilon_{p-1} + \varepsilon'_{p-1}, \tau_p)$, while $[\tau_p, \tau_p + \varepsilon_p)$ and $[\tau_p + \varepsilon_p, \tau_p + \varepsilon_p + \varepsilon'_p)$, respectively, represent two intervals in which a shock to the standby system takes place and the subsequent responses of the monitoring subsystem, switching device and warm standby occur in this system. Notice also that ε'_p ($p = 0, 1, 2, \cdots$) should be considered as two very short (approaching zero) time periods. To simplify analysis, it is assumed in this study that the probability of two or more instrument faults occurring in $[\tau_p + \varepsilon_p, \tau_p + \varepsilon_p + \varepsilon'_p)$ is extremely low and can be realistically neglected. In addition, although there may be fail-safe (FS) and fail-dangerous (FD) sensor malfunctions, it is assumed in this study that the former can be eliminated via a proper filtering technique. In other words, the response to steady load during operation can only result in the same judgment according to the online measurements.

Figures 3−6 show the event trees for Mode I, Mode I^0, Mode II, and Mode II^0, respectively. Notice first that the boundary time points of the aforementioned different intervals in which various critical events may occur are marked at the top of each figure. It can be observed that the paths in these trees during the time interval $[\tau_p + \varepsilon_p, \tau_p + \varepsilon_p + \varepsilon'_p)$ are color-coded. A black branch denotes the corresponding component is normal. The blue branches represent components experiencing FS failures, while the red ones represent the corresponding components failed dangerously. It can also be seen that a label is placed at the tip of each branch of every event tree to distinguish the corresponding scenario from the others. Scenarios O, A, and B are caused by load decrease, load increase, and online unit failure, respectively, under the condition that the standby mechanism functions properly; Scenarios −1 and 0 (labeled with black color) result in no losses; Scenarios 1−3, 5, and 6 (labeled with blue color) result in the "supply-larger-than-demand" losses; Scenarios 4 and 7−15 (labeled with red color) result in the "supply-smaller-than-demand" losses. In other words, the financial losses caused by abnormal components in a standby system are classified into the above two types in this study. The former is used to represent the abnormal condition of the given system which causes the production rate of the protected online unit exceeding the actual load, while the latter ends up with the undesirable situation of online supply rate not enough for satisfying demand.

Also, notice that various binary or ternary variables are stipulated under the branches of every event tree. The binary variable ξ_l is used to represent whether the lth online unit is functional ($\xi_l = 0$) or failed ($\xi_l = 1$); the ternary variable π_l characterizes three possible scenarios, i.e., load decrease when the lth unit is running online ($\pi_l = -1$), load unchanged when the lth unit is running online ($\pi_l = 0$) and load decrease when the lth unit is running online ($\pi_l = -1$); the binary variable w represents the outcome of applying OR operation to the outputs of all α measurement channels, i.e., the corresponding monitoring subsystem detects a load change ($w = 1$) or otherwise ($w = 0$); the binary variable q_l represents the outcome of applying OR operation to the outputs of all β monitoring channels, i.e., $q_l = 1$ implies that the standby system output does not match demand and the switching device is supposed to send a signal to turn on a warm standby or to shut down an online unit

https://doi.org/10.1021/acs.iecr.2c04521
Ind. Eng. Chem. Res. 2023, 62, 5150−5169

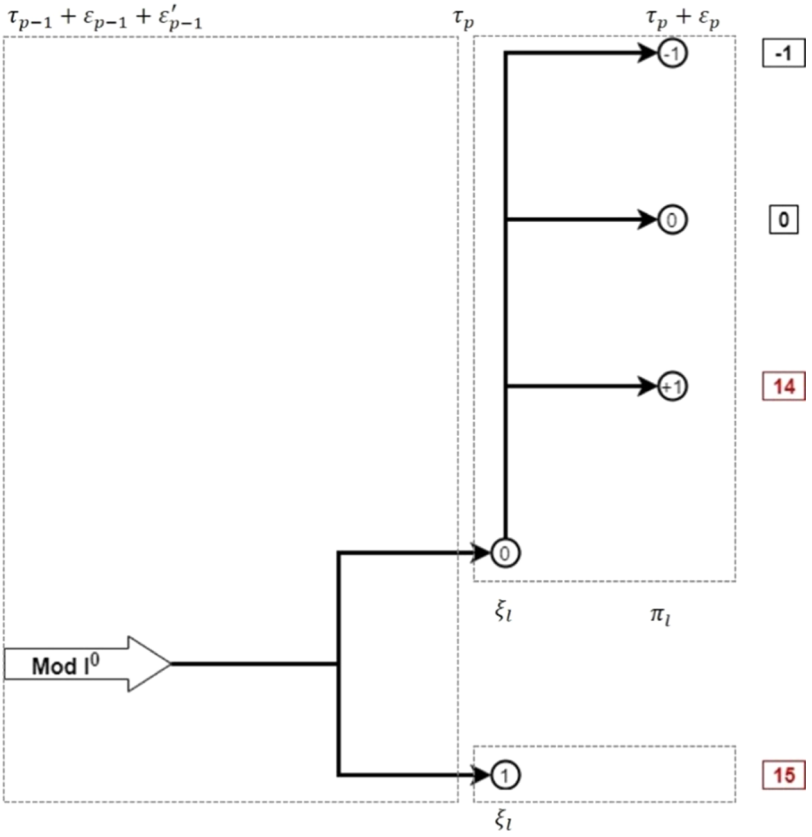

Figure 4. Event tree for Mode I^0.

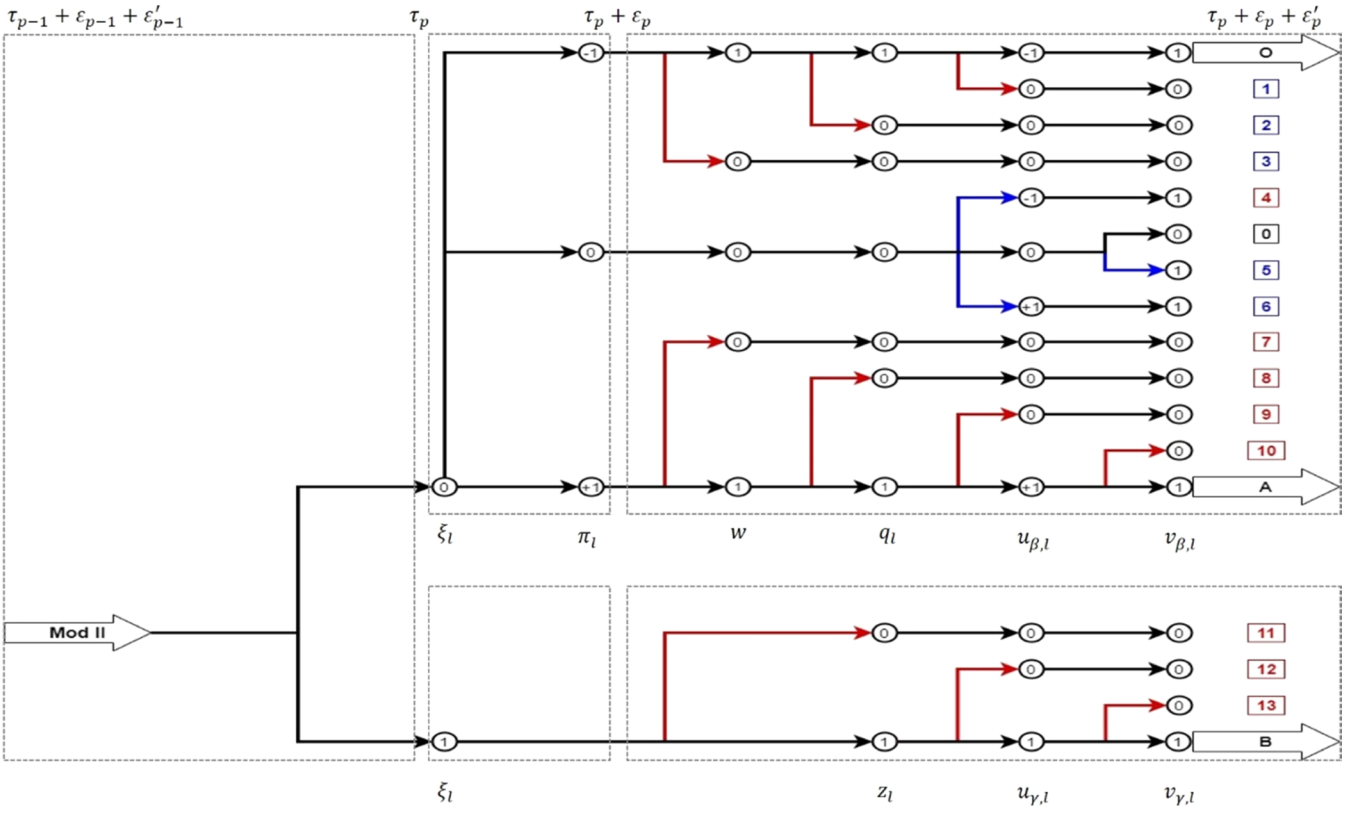

Figure 5. Event tree for Mode II.

and q_l = 0 means that the standby system output matches demand and the switching device is supposed to do nothing; the ternary variable $u_{\beta,l}$ is used to further differentiate the above switching signals, i.e., command to move a unit from online to

https://doi.org/10.1021/acs.iecr.2c04521
Ind. Eng. Chem. Res. 2023, 62, 5150−5169

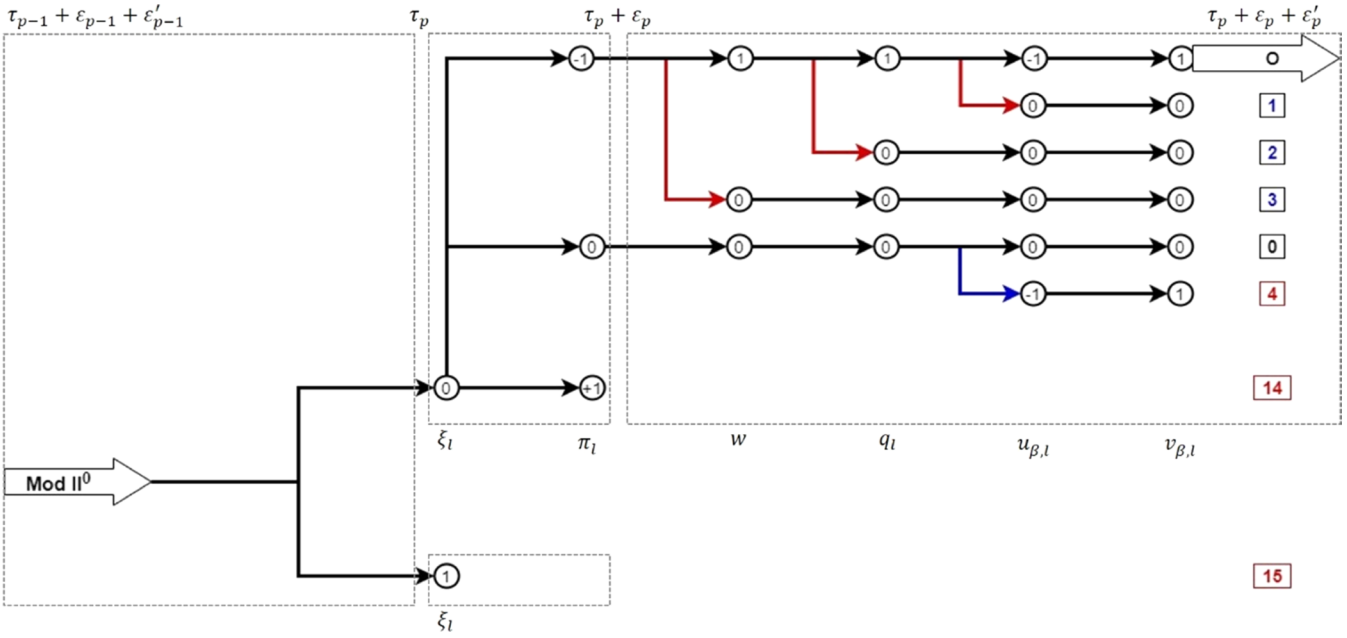

Figure 6. Event tree for Mode II^0.

warm standby when the lth unit is running ($u_{\beta,l} = -1$), command to move a unit from warm standby to online when the lth unit is running online ($u_{\beta,l} = +1$), and keep system configuration unchanged ($u_{\beta,l} = 0$); the binary variable $v_{\beta,l}$ is introduced to indicate whether or not the standby system responds correctly when the lth unit is running under load change, i.e., $v_{\beta,l} = 1$ is used to reflect the former (correct) action and $v_{\beta,l} = 0$ indicates otherwise; the binary variable z_l is adopted to represent the outcome of applying the OR operation to sensor measurements in all γ monitoring channels, i.e., the $(l+1)$th unit (that is, the lth warm standby) should be switched on if $z_l = 1$ and otherwise if $z_l = 0$; the binary variable $u_{\gamma,l}$ is used to represent whether the switching device functions properly at the time when it is needed, i.e., the switch acts correctly in accordance with OR logic when $u_{\gamma,l} = 1$ and otherwise when $u_{\gamma,l} = 0$; the binary variable $v_{\gamma,l}$ is used to indicate whether the lth warm standby responds as expected, i.e., the lth warm standby responds correctly when an online unit fails if $v_{\gamma,l} = 1$ and otherwise when $v_{\gamma,l} = 0$. Notice that the labels of α, β, and γ monitoring subsystems were assigned for convenience in this study, and they were adopted simply to differentiate different groups of sensors to detect load changes, supply−demand mismatches, and processing unit failures, respectively. Finally, it is important to note that the integer values of the aforementioned variables are specified in the nodes located directly above each of them and the more in-depth descriptions of the superstructure and the corresponding variables can be found in Part A of the SI file.

Before going into more detailed discussions, there are still a few details that must be provided to facilitate better explanations of the event trees.

- It is assumed in this study that at most one equipment malfunction, i.e., FS or FD failures of monitoring subsystems, switching device, or warm standbys, may take place during interval $[\tau_p + \varepsilon_p, \tau_p + \varepsilon_p + \varepsilon'_p)$ in every scenario.
- Since it is also required that at least one processing unit in the standby system should be kept running online, the option of -1 of ternary variable $u_{\gamma,l}$ is excluded in the event tree of Mode I in Figure 3. For the same reason, there are no responses for $\pi_l = -1$ (i.e., the event of load decrease) in this event tree since only one online unit is running in this case.
- The event tree of Mode I^0 in Figure 4 is used to enumerate the scenarios after all warm standbys have been out of order. If a further event of load increase (scenario 14) or online unit failure (scenario 15) takes place, the supply-smaller-than-demand loss is inevitable since Mode I^0 reaches a condition with no standby protection.
- If the measurements of monitoring channels call for removal of an online unit in response to a detected load-decrease signal and, at the same time, the switching device functions correctly, it is assumed in this situation that the malfunction of the above-mentioned online unit, i.e., it fails to act accordingly, is improbable. Therefore, in the event trees of Mode II in Figure 5 and Mode II^0 in Figure 6, when a command is issued to transfer the state of a unit from online to warm standby, i.e., $u_{\gamma,l} = -1$, the system always acts accordingly, i.e., $u_{\gamma,l} = 1$. This behavior can be found in scenario O and scenario 4.
- After an online unit fails, i.e., $\xi_l = 1$, the subsequent FS failures of the monitoring subsystem, the switching device, and the warm standby should all be excluded from consideration (see Figures 3 and 5). This is because of the fact that these FS failures lack physical significance.
- Since the system is not equipped with warm standby in Mode II^0, the ternary variable $u_{\gamma,l}$ is devoid of the option of +1 in the corresponding event tree in Figure 6. In addition, in cases of load increase and online unit failure, a supply-smaller-than-demand loss is bound to occur (scenarios 14 and 15). Finally, when a command is issued to keep the current system configuration, i.e., $u_{\gamma,l} = 0$, there is no chance for the FS failure, i.e., to transfer a warm standby state to online state, and the value of $v_{\gamma,l}$ is always zero.

Notice that the improbable branches in the aforementioned four events trees in Figures 3−6 have already been eliminated for

https://doi.org/10.1021/acs.iecr.2c04521
Ind. Eng. Chem. Res. 2023, 62, 5150−5169

the sake of clarity. Furthermore, the detailed descriptions of every scenario in each event tree are placed in Part B in the SI to facilitate illustrative clarity.

4. COMPONENT MODELS

To construct a rigorous programming model for generating optimal design of the standby system, the reliability model of every component should be formulated in advance.

Let us first consider the online unit(s) in the superstructure. As mentioned before, an online unit may experience three types of shocks, i.e., load increase, load decrease, and mechanical failure. It is assumed in this study that these events take place independently that mimic three different homogeneous Poisson processes, respectively.[26] The shock intensities of load increase and decrease are denoted as λ_+ (year^{-1}) and λ_- (year^{-1}), respectively, while that of a single online unit failure is $\lambda_{f,\text{single}}$ (year^{-1}). Since there may be several (say n) units running simultaneously, their overall failure intensity λ_f can be expressed as.

$$\lambda_f = n\lambda_{f,\text{single}} \tag{1}$$

The number of online units (n) in a configuration associated with the entry at the rth row and cth column of the structural transformation matrix (see Figure 1) can be determined as follows

$$n = c - r + 1 \tag{2}$$

Let us then denote the lumped shock intensity of the above-mentioned all events to be λ,i.e.,

$$\lambda = \lambda_+ + \lambda_- + \lambda_f \tag{3}$$

Next use T_p^f, T_p^+ and T_p^- to represent respectively the time intervals between the pth and $(p-1)$th shocks. Since $0 < \tau_{p-1} < t \le H$, the probabilities of mechanical failure, load increase, and decrease in interval $(\tau_{p-1},t]$ (which are denoted in the sequel as $\Phi_{T_p^f}$, $\Phi_{T_p^+}$, and $\Phi_{T_p^-}$, respectively) can be expressed as

$$\begin{aligned}\Phi_{T_p^f}(t) &= \Pr\{(T_p^f < t - \tau_{p-1} < T_p^+) \wedge (T_p^f < t - \tau_{p-1} < T_p^-)\} \\ &= \left[\frac{\lambda_f}{\lambda}\right][1 - e^{-\lambda(t-\tau_{p-1})}]\end{aligned} \tag{4}$$

$$\begin{aligned}\Phi_{T_p^+}(t) &= Pr\{(T_p^+ < t - \tau_{p-1} < T_p^f) \wedge (T_p^+ < t - \tau_{p-1} < T_p^-)\} \\ &= \left[\frac{\lambda_+}{\lambda}\right][1 - e^{-\lambda(t-\tau_{p-1})}]\end{aligned} \tag{5}$$

$$\begin{aligned}\Phi_{T_p^-}(t) &= Pr\{(T_p^- < t - \tau_{p-1} < T_p^f) \wedge (T_p^- < t - \tau_{p-1} < T_p^+)\} \\ &= \left[\frac{\lambda_-}{\lambda}\right][1 - e^{-\lambda(t-\tau_{p-1})}]\end{aligned} \tag{6}$$

Thus, the probability of no shocks in $(\tau_{p-1},t]$ can be written as

$$\begin{aligned}&Pr\{(T_p^f > t - \tau_{p-1}) \wedge (T_p^+ > t - \tau_{p-1}) \wedge (T_p^- > t - \tau_{p-1})\} \\ &= 1 - \Phi_{T_p^f}(t) - \Phi_{T_p^+}(t) - \Phi_{T_p^-}(t) \\ &= e^{-\lambda(t-\tau_{p-1})}\end{aligned} \tag{7}$$

According to the event trees presented in Figures 3−6, any shock may take place in interval $(\tau_p, \tau_p + \varepsilon_p]$ within period (τ_{p-1},t). Since $\varepsilon_p \to 0$, this interval can also be rewritten as $(\tau_p, \tau_p + d\tau_p]$ and the probabilities of the aforementioned three types of shocks occurring in this instance can be expressed respectively as follows

$$Pr\{\xi_l(\tau_p) = 1\} = \left.\frac{d\Phi_{T_p^f}(t)}{dt}\right|_{t=\tau_p} d\tau_p = \lambda_f e^{-\lambda(\tau_p - \tau_{p-1})} d\tau_p \tag{8}$$

$$Pr\{\pi_l(\tau_p) = +1\} = \left.\frac{d\Phi_{T_p^+}(t)}{dt}\right|_{t=\tau_p} d\tau_p = \lambda_+ e^{-\lambda(\tau_p - \tau_{p-1})} d\tau_p \tag{9}$$

$$Pr\{\pi_l(\tau_p) = -1\} = \left.\frac{d\Phi_{T_p^-}(t)}{dt}\right|_{t=\tau_p} d\tau_p = \lambda_- e^{-\lambda(\tau_p - \tau_{p-1})} d\tau_p \tag{10}$$

The probability expressions for fail-safe and fail-dangerous events of all other components in the superstructure are placed in Part C and Part D of the SI for brevity's sake.

5. SCENARIO PROBABILITIES

With the structural transformation matrix in Figure 1 and the event trees in Figures 3−6, one can enumerate all possible event sequences in the standby system exhaustively. In this section, a generalized mathematical model is rigorously derived so as to determine the probability of every scenario over the entire operation horizon that may result in a significant loss. The total lifecycle expected loss can then be calculated according to these probabilities.

The structural transformation matrix (Figure 1) shows that, in principle, the standby system may go through an infinite number of repeated load increase(s) and load decrease(s) within a finite time period. To be realistic, a simplified approach is taken in this study to obtain a practical estimate of the average number of load decreases over the operation horizon. Specifically, since the shock intensity λ_- can be interpreted as the mean value of the number of load decreases per unit time, the above number estimate (denoted as R) can be expressed as

$$R = \lambda_- \times H \tag{11}$$

On the other hand, it should be noted that Figure 1 is essentially a folded representation of the evolution process of system configurations over time. From the column and row numbers of an entry in the structural transformation matrix, one can only depict the corresponding system configuration without knowing its evolution history. To identify all possible fault propagation scenarios, it is necessary to integrate the information embedded in the structural transformation matrix in Figure 1 and the event trees in Figures 3−6. To this end, let us assign each scenario a four-number identification code, i.e., $r\_c\_p\_s$. In this code, r and c can be used to identify the location of a standby system in the structural transformation matrix, i.e., r and c denote the row and column numbers, respectively; p represents the number of shocks experienced by the standby system; and s is the scenario number in the event tree which corresponds to the configuration at the rth row and cth column in the structural transformation matrix. From Figures 3−6, one can see that

- scenarios 1−15 in the four event trees all result in financial losses.
- scenario O, A, or B facilitates the transfer of one configuration (block) to another.

https://doi.org/10.1021/acs.iecr.2c04521
Ind. Eng. Chem. Res. 2023, 62, 5150−5169

For this reason, the probabilities of the latter three scenarios are referred to as the connective terms of a block in the present study.

Based on the above discussions, it can be deduced that the standby system may experience a total of $\left\{(R+1)\left[2+15(L+1)+\frac{13}{2}(L-1)(L-2)\right]\right\}$ different scenarios that result in losses. Let us consider a specific standby system as an example for clearer illustration of the derivation process of a mathematical model. The structural transformation matrix corresponding to $L = 4$ and $R > 0$ can be first constructed as that shown in Figure 7. Notice that each block in this diagram

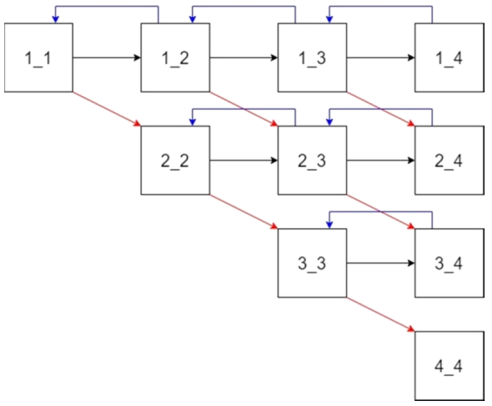

Figure 7. Structural transformation matrix showing all structure-to-structure transition routes for $L = 4$ and $R > 0$.

is inscribed with the condensed identification code r_c. As mentioned before, $r - 1$ is the number of failed units and c is the total number of units not taken offline. Also, the blue, black, and red arrows are used to represent the transformation paths from one configuration to the next via scenarios O, A, and B, respectively, in the event tree corresponding to the upstream block. If $R = 2$, then the matrix in Figure 7 can be expanded to form the three upper triangular matrices in Figure 8 by considering the precedence order of the shocks. Notice first that the probability of initial normal state is assumed to be always present, i.e., 1, is placed in the circle located at the far left of Figure 8. The three-number identification code given in each block of the expanded structural transformation matrices, i.e., r_c_p, is used to assign numerical labels of corresponding row (r), column (c), and shock (p). Also, notice that the total number of upper triangular matrices should be $R + 1$, where R can be determined according to eq 11.

Let us consider the first row of the first upper-triangular submatrix in Figure 8, and derive the mathematical expressions of probabilities of every scenario contained herein using the previously defined notation $P_{r\_c\_p\_s}$. The first block in the above-mentioned row is labeled as 1_1_1 (see Figure 8), and the event tree associated with this block should be described with Mode I in Figure 3. The probability of the fifth scenario in the corresponding event tree can be determined as follows.

$$P_{1\_1\_1\_5}(t) = \int_0^t [e^{-\lambda\tau_1}][1 - PFS_{sw}(\tau_1)][c_{wb}]\mathrm{d}\tau_1 \tag{12}$$

Differentiating $P_{1\_1\_1\_5}(t)$ with respect to time according to the Leibniz rule yields

$$\dot{P}_{1\_1\_1\_5}(t) = [e^{-\lambda t}][1 - PFS_{sw}(t)][c_{wb}] \tag{13}$$

By following the same derivation, the probabilities of all other scenarios in the event tree associated with block 1_1_1 can be obtained and their derivatives are listed below:

$$\dot{P}_{1\_1\_1\_6}(t) = [e^{-\lambda t}][c_{sw}(t)][1 - PFD_{wb}(t)] \tag{14}$$

$$\dot{P}_{1\_1\_1\_7}(t) = [\lambda_+ e^{-\lambda t}][PFD_{sr\alpha}(t)][1 - PFS_{sw}(t)][1 - PFS_{wb}(t)] \tag{15}$$

$$\dot{P}_{1\_1\_1\_8}(t) = [\lambda_+ e^{-\lambda t}][1 - PFD_{sr\alpha}(t)][PFD_{sr\beta}(t)][1 - PFS_{sw}(t)][1 - PFS_{wb}(t)] \tag{16}$$

$$\dot{P}_{1\_1\_1\_9}(t) = [\lambda_+ e^{-\lambda t}][1 - PFD_{sr\alpha}(t)][1 - PFD_{sr\beta}(t)][PFD_{sw}(t)][1 - PFS_{wb}(t)] \tag{17}$$

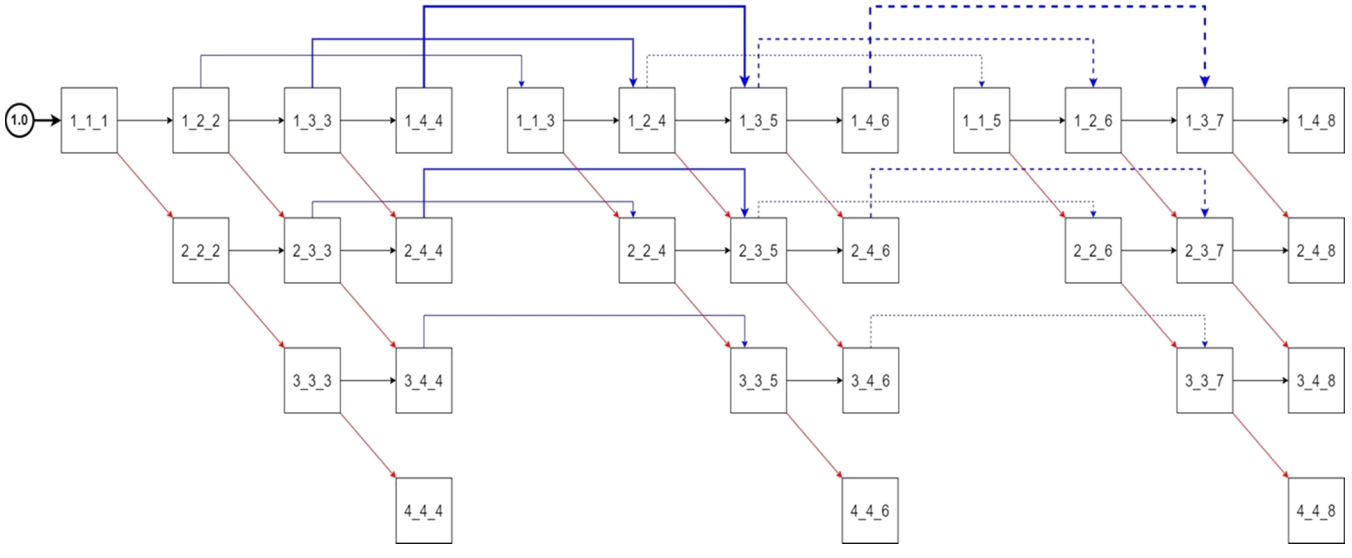

Figure 8. Structural transformation matrices expanded from Figure 7 by considering shocks for $L = 4$ and $R = 2$.

https://doi.org/10.1021/acs.iecr.2c04521
Ind. Eng. Chem. Res. 2023, 62, 5150−5169

$$\dot{P}_{1\_1\_1\_10}(t) = [\lambda_{+}e^{-\lambda t}][1 - PFD_{sr\alpha}(t)][1 - PFD_{sr\beta}(t)] [1 - PFD_{sw}(t)][PFD_{wb}(t)] \quad (18)$$

$$\dot{P}_{1\_1\_1\_11}(t) = [\lambda_{f}e^{-\lambda t}][PFD_{sr\gamma}(t)][1 - PFS_{sw}(t)] [1 - PFS_{wb}(t)] \quad (19)$$

$$\dot{P}_{1\_1\_1\_12}(t) = [\lambda_{f}e^{-\lambda t}][1 - PFD_{sr\gamma}(t)][PFD_{sw}(t)] [1 - PFS_{wb}(t)] \quad (20)$$

$$\dot{P}_{1\_1\_1\_13}(t) = [\lambda_{f}e^{-\lambda t}][1 - PFD_{sr\gamma}(t)][1 - PFD_{sw}(t)] [PFD_{wb}(t)] \quad (21)$$

$$\dot{P}_{1\_1\_1\_A}(t) = [\lambda_{+}e^{-\lambda t}][1 - PFD_{sr\alpha}(t)][1 - PFD_{sr\beta}(t)] [1 - PFD_{sw}(t)][1 - PFD_{wb}(t)] \quad (22)$$

$$\dot{P}_{1\_1\_1\_B}(t) = [\lambda_{f}e^{-\lambda t}][1 - PFD_{sr\gamma}(t)][1 - PFD_{sw}(t)] [1 - PFD_{wb}(t)] \quad (23)$$

Block 1_1_1 is transformed into block 1_2_2 via scenario 1_1_1_*A*. A few examples of the resulting probabilities and their derivatives for scenarios 1_2_2_*s* are presented as follows

$$\begin{aligned} P_{1\_2\_2\_1}(t) &= \int_0^t \int_0^{\tau_2} \dot{P}_{1\_1\_1\_A}(\tau_1)[\lambda\_e^{-\lambda(\tau_2-\tau_1)}] [1 - PFD_{sr\alpha}(\tau_2)][1 - PFD_{sr\beta}(\tau_2)] [PFD_{sw}(\tau_2)][1 - PFS_{wb}(\tau_2)]\mathrm{d}\tau_1\mathrm{d}\tau_2 \\ &= \int_t^0 [\lambda\_e^{-\lambda\tau_2}][1 - PFD_{sr\alpha}(\tau_2)] [1 - PFD_{sr\beta}(\tau_2)][PFD_{sw}(\tau_2)] [1 - PFS_{wb}(\tau_2)] \int_{\tau_2}^0 \dot{P}_{1\_1\_1\_A}(\tau_1) e^{\lambda\tau_1}\mathrm{d}\tau_1\mathrm{d}\tau_2 \end{aligned} \quad (24)$$

$$\begin{aligned} \dot{P}_{1\_2\_2\_1}(t) &= \int_0^t \dot{P}_{1\_1\_1\_A}(\tau_1)e^{\lambda\tau_1}[\lambda\_e^{-\lambda t}][1 - PFD_{sr\alpha}(t)] [1 - PFD_{sr\beta}(t)][PFD_{sw}(t)][1 - PFS_{wb}(t)] \mathrm{d}\tau_1 \\ &= [\lambda\_e^{-\lambda t}][1 - PFD_{sr\alpha}(t)][1 - PFD_{sr\beta}(t)] [PFD_{sw}(t)][1 - PFS_{wb}(t)]P^*_{1\_1\_1\_A}(t) \end{aligned} \quad (25)$$

$$\dot{P}_{1\_2\_2\_O}(t) = [\lambda\_e^{-\lambda t}][1 - PFD_{sr\alpha}(t)][1 - PFD_{sr\beta}(t)] [1 - PFD_{sw}(t)]P^*_{1\_1\_1\_A}(t) \quad (26)$$

$$\dot{P}_{1\_2\_2\_A}(t) = [\lambda_{+}e^{-\lambda t}][1 - PFD_{sr\alpha}(t)][1 - PFD_{sr\beta}(t)] [1 - PFD_{sw}(t)][1 - PFD_{wb}(t)]P^*_{1\_1\_1\_A}(t) \quad (27)$$

$$\dot{P}_{1\_2\_2\_B}(t) = [\lambda_{f}e^{-\lambda t}][1 - PFD_{sr\gamma}(t)][1 - PFD_{sw}(t)] [1 - PFD_{wb}(t)]P^*_{1\_1\_1\_A}(t) \quad (28)$$

where

$$P^*_{1\_1\_1\_A}(t) = \int_0^t \dot{P}_{1\_1\_1\_A}(\tau_1)e^{\lambda\tau_1}\mathrm{d}\tau_1 \quad (29)$$

$$\dot{P}^*_{1\_1\_1\_A}(t) = \dot{P}_{1\_1\_1\_A}(t)e^{\lambda t} \quad (30)$$

For the sake of brevity, the complete list of probability derivatives for all scenarios in block 1_2_2 is moved to Part E in SI.

Next, notice that the passage from block 1_2_2 to block 1_3_3 is through scenario 1_2_2_*A*. A few examples of the probabilities and their derivatives for scenarios 1_3_3_*s* are listed below

$$P_{1\_3\_3\_1}(t) = \int_0^t [\lambda\_e^{-\lambda\tau_3}][1 - PFD_{sr\alpha}(\tau_3)][1 - PFD_{sr\beta}(\tau_3)] [PFD_{sw}(\tau_3)][1 - PFS_{wb}(\tau_3)]P^*_{1\_2\_2\_A}(\tau_3)\mathrm{d}\tau_3 \quad (31)$$

$$\dot{P}_{1\_3\_3\_1}(t) = [\lambda\_e^{-\lambda t}][1 - PFD_{sr\alpha}(t)][1 - PFD_{sr\beta}(t)] [PFD_{sw}(t)][1 - PFS_{wb}(t)]P^*_{1\_2\_2\_A}(t) \quad (32)$$

where

$$\begin{aligned} P^*_{1\_2\_2\_A}(t) &= \int_0^t [\lambda_{+}e^{-\lambda\tau_2}][1 - PFD_{sr\alpha}(\tau_2)] [1 - PFD_{sr\beta}(\tau_2)][1 - PFD_{sw}(\tau_2)] [1 - PFD_{wb}(\tau_2)]e^{\lambda\tau_2} \int_0^{\tau_2} \dot{P}_{1\_1\_1\_A}(\tau_1) e^{\lambda\tau_1}\mathrm{d}\tau_1\mathrm{d}\tau_2 \\ &= \int_0^t [\lambda_{+}e^{-\lambda\tau_2}][1 - PFD_{sr\alpha}(\tau_2)] [1 - PFD_{sr\beta}(\tau_2)][1 - PFD_{sw}(\tau_2)] [1 - PFD_{wb}(\tau_2)]e^{\lambda\tau_2}P^*_{1\_1\_1\_A}(\tau_2)\mathrm{d}\tau_2 \end{aligned} \quad (33)$$

and

$$\begin{aligned} \dot{P}^*_{1\_2\_2\_A}(t) &= [\lambda_{+}e^{-\lambda t}][1 - PFD_{sr\alpha}(t)][1 - PFD_{sr\beta}(t)] [1 - PFD_{sw}(t)][1 - PFD_{wb}(t)]e^{\lambda t} P^*_{1\_1\_1\_A}(t) \\ &= \dot{P}_{1\_2\_2\_A}(t)e^{\lambda t} \end{aligned} \quad (34)$$

The complete list of probability derivatives for all scenarios in block 1_3_3 is also provided in Part E in the SI for the sake of brevity.

Finally, it can also be observed that the link between block 1_3_3 and block 1_4_4 is scenario 1_3_3_*A*. A few examples of the probabilities and their derivatives for scenarios 1_4_4_*s* can be found below

$$P_{1\_4\_4\_1}(t) = \int_0^t [\lambda\_e^{-\lambda\tau_4}][1 - PFD_{sr\alpha}(\tau_4)][1 - PFD_{sr\beta}(\tau_4)] [PFD_{sw}(\tau_4)]P^*_{1\_3\_3\_A}(\tau_4)\mathrm{d}\tau_4 \quad (35)$$

$$\dot{P}_{1\_4\_4\_1}(t) = [\lambda\_e^{-\lambda t}][1 - PFD_{sr\alpha}(t)][1 - PFD_{sr\beta}(t)] [PFD_{sw}(t)][1 - PFS_{wb}(t)]P^*_{1\_3\_3\_A}(t) \quad (36)$$

where

https://doi.org/10.1021/acs.iecr.2c04521
Ind. Eng. Chem. Res. 2023, 62, 5150−5169

$$P^*_{1\_3\_3\_A}(t) = \int_0^t [\lambda_+ e^{-\lambda\tau_3}][1 - PFD_{sr\alpha}(\tau_3)][1 - PFD_{sr\beta}(\tau_3)] [1 - PFD_{sw}(\tau_3)][1 - PFD_{wb}(\tau_3)]e^{\lambda\tau_3} P^*_{1\_2\_2\_A}(\tau_3)\mathrm{d}\tau_3 \quad (37)$$

and

$$\dot{P}^*_{1\_3\_3\_A}(t) = [\lambda_+ e^{-\lambda t}][1 - PFD_{sr\alpha}(t)][1 - PFD_{sr\beta}(t)] [1 - PFD_{sw}(t)][1 - PFD_{wb}(t)]e^{\lambda t} P^*_{1\_2\_2\_A}(t) = \dot{P}_{1\_3\_3\_A}(t)e^{\lambda t} \quad (38)$$

Again, the complete list of probability derivatives for all scenarios in block 1_4_4 is placed in Part E in the SI for the sake of brevity.

From eqs 12−38 and Part E in the SI, it can be observed that the expression for probability derivative of each scenario consists of two groups of formulations, i.e., a probability density function and a so-called connective term mentioned previously.

- Probability density function: This expression type is used to characterize the shock and the subsequent system responses, which is associated with the scenario (s = 1, 2, ⋯, 15, O, A, B) corresponding to the tree branches in Figures 3−6. For formulation simplicity and convenience, this function is denoted as $f_s(t)$ throughout this paper and all such functions are listed below

$$f_1(t) = \begin{cases} [\lambda\_e^{-\lambda t}][1 - PFD_{sr\alpha}(t)][1 - PFD_{sr\beta}(t)] [PFD_{sw}(t)]; & c = L \\ [\lambda\_e^{-\lambda t}][1 - PFD_{sr\alpha}(t)][1 - PFD_{sr\beta}(t)] [PFDsw(t)][1 - PFS_{wb}(t)]; & c < L \end{cases} \quad (39)$$

$$f_2(t) = \begin{cases} [\lambda\_e^{-\lambda t}][1 - PFD_{sr\alpha}(t)][PFD_{sr\beta}(t)] [1 - PFS_{sw}(t)]; & c = L \\ [\lambda\_e^{-\lambda t}][1 - PFD_{sr\alpha}(t)][PFD_{sr\beta}(t)] [1 - 2PFS_{sw}(t)][1 - PFS_{wb}(t)]; & c < L \end{cases} \quad (40)$$

$$f_4(t) = [e^{-\lambda t}][c_{sw}(t)] \quad (42)$$

$$f_5(t) = \begin{cases} [e^{-\lambda t}][1 - PFS_{sw}(t)][c_{wb}(t)]; & \text{ModeI} \\ [e^{-\lambda t}][1 - 2PFS_{sw}(t)][c_{wb}(t)]; & \text{ModeII} \end{cases} \quad (43)$$

$$f_6(t) = [e^{-\lambda t}][c_{sw}(t)][1 - PFD_{wb}(t)] \quad (44)$$

$$f_7(t) = \begin{cases} [\lambda_+ e^{-\lambda t}][PFD_{sr\alpha}(t)][1 - PFS_{sw}(t)] [1 - PFS_{wb}(t)]; & \text{ModeI} \\ [\lambda_+ e^{-\lambda t}][PFD_{sr\alpha}(t)][1 - 2PFS_{sw}(t)] [1 - PFS_{wb}(t)]; & \text{ModeII} \end{cases} \quad (45)$$

$$f_8(t) = \begin{cases} [\lambda_+ e^{-\lambda t}][1 - PFD_{sr\alpha}(t)][PFD_{sr\beta}(t)] [1 - PFS_{sw}(t)][1 - PFS_{wb}(t)]; & \text{ModeI} \\ [\lambda_+ e^{-\lambda t}][1 - PFD_{sr\alpha}(t)][PFD_{sr\beta}(t)] [1 - 2PFS_{sw}(t)][1 - PFS_{wb}(t)]; & \text{ModeII} \end{cases} \quad (46)$$

$$f_9(t) = [\lambda_+ e^{-\lambda t}][1 - PFD_{sr\alpha}(t)][1 - PFD_{sr\beta}(t)][PFD_{sw}(t)] [1 - PFS_{wb}(t)] \quad (47)$$

$$f_{10}(t) = [\lambda_+ e^{-\lambda t}][1 - PFD_{sr\alpha}(t)][1 - PFD_{sr\beta}(t)] [1 - PFD_{sw}(t)][PFD_{wb}(t)] \quad (48)$$

$$f_{11}(t) = [\lambda_f e^{-\lambda t}][PFD_{sr\gamma}(t)][1 - PFS_{sw}(t)][1 - PFS_{wb}(t)] \quad (49)$$

$$f_{12}(t) = [\lambda_f e^{-\lambda t}][1 - PFD_{sr\gamma}(t)][PFD_{sw}(t)][1 - PFS_{wb}(t)] \quad (50)$$

$$f_{13}(t) = [\lambda_f e^{-\lambda t}][1 - PFD_{sr\gamma}(t)][1 - PFD_{sw}(t)][PFD_{wb}(t)] \quad (51)$$

$$f_{14}(t) = [\lambda_+ e^{-\lambda t}] \quad (52)$$

$$f_{15}(t) = [\lambda_f e^{-\lambda t}] \quad (53)$$

$$f_O(t) = [\lambda\_e^{-\lambda t}][1 - PFD_{sr\alpha}(t)][1 - PFD_{sr\beta}(t)] [1 - PFD_{sw}(t)] \quad (54)$$

$$f_A(t) = [\lambda_+ e^{-\lambda t}][1 - PFD_{sr\alpha}(t)][1 - PFD_{sr\beta}(t)] [1 - PFD_{sw}(t)][1 - PFD_{wb}(t)] \quad (55)$$

$$f_B(t) = [\lambda_f e^{-\lambda t}][1 - PFD_{sr\gamma}(t)][1 - PFD_{sw}(t)] [1 - PFD_{wb}(t)] \quad (56)$$

- Connective terms: Three connective terms are used to indicate the incoming paths via which the current system configuration takes shape. They can be adopted to trace the history of previous shocks and the corresponding responses before the present state. These terms are denoted as $P^*_{r\_c\_p\_O}$, $P^*_{r\_c\_p\_A}$, and $P^*_{r\_c\_p\_B}$, respectively, and they and their derivatives are given below

$$P^*_{r\_c\_p\_O}(t) = \int_0^t e^{\lambda\tau_p}\dot{P}_{r\_c\_p\_O}(\tau_p)\mathrm{d}\tau_p \quad (57)$$

$$\dot{P}^*_{r\_c\_p\_O}(t) = e^{\lambda t}\dot{P}_{r\_c\_p\_O}(t) \quad (58)$$

$$P^*_{r\_c\_p\_A}(t) = \int_0^t e^{\lambda\tau_p}\dot{P}_{r\_c\_p\_A}(\tau_p)\mathrm{d}\tau_p \quad (59)$$

$$\dot{P}^*_{r\_c\_p\_A}(t) = e^{\lambda t}\dot{P}_{r\_c\_p\_A}(t) \quad (60)$$

$$P^*_{r\_c\_p\_B}(t) = \int_0^t e^{\lambda\tau_p}\dot{P}_{r\_c\_p\_B}(\tau_p)\mathrm{d}\tau_p \quad (61)$$

$$\dot{P}^*_{r\_c\_p\_B}(t) = e^{\lambda t}\dot{P}_{r\_c\_p\_B}(t) \quad (62)$$

https://doi.org/10.1021/acs.iecr.2c04521
Ind. Eng. Chem. Res. 2023, 62, 5150−5169

As mentioned before, eqs 12−38 and Part E in the SI are concerned only with the first row of blocks in the first upper-triangular matrix in Figure 8. It is obviously necessary to determine the probabilities of all other scenarios in the expanded structural transformation matrix. It can be observed from Figure 8 that, except block 1_1_1, every configuration (block) is affected via at least one out of three routes and the corresponding connective terms are $P^*_{r\_c\_p\_O}$, $P^*_{r\_c\_p\_A}$ and $P^*_{r\_c\_p\_B}$.

Let us next consider the precursors and their corresponding connective terms that lead to a particular configuration (say r_c_p). As mentioned before, p is the serial number of shocks (load increase, load decrease, or mechanical failure) and, thus, this number for the precursors should be $p - 1$; The column label c represents the total number of units not taken offline (including those currently in use and also the failed ones). If the event of load increase or online unit failure takes place in the precursor block, then its column label should be $c - 1$. If the event of load decrease occurs in the precursor, then this label becomes $c + 1$; Finally, notice that the row label minus one, i.e., $r - 1$, equals the number of broken units. Therefore, the shocks of load changes in the precursor do not alter the row label after transforming into configuration r_c_p. On the other hand, if online unit failure takes place in the precursor, then its own row label should be one less than that in the configuration after shock. Based on the above discussions, one can summarize all connection routes leading to a particular destination, i.e., configuration r_c_p, with Figure 9.

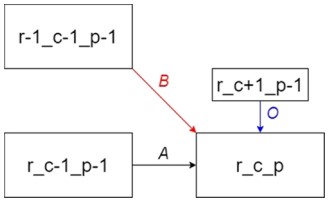

Figure 9. Connection routes leading to configuration r_c_p.

On the basis of the connection routes depicted in Figure 9 and eqs 39−62, a single generalized equation can be constructed for characterizing probability derivatives associated with all possible scenarios in the expanded structural transformation matrix. Specifically,

$$\dot{P}_{r\_c\_p\_s}(t) = f_s(t)[P^*_{r\_(c+1)\_(p-1)\_O}(t) + P^*_{r\_(c-1)\_(p-1)\_A}(t) + P^*_{(r-1)\_(c-1)\_(p-1)\_B}(t)] \quad (63)$$

Notice that equations 39−56 can be utilized to determine $f_s(t)$ (s = 1, 2, ⋯, 15, O, A, B), eqs 57 or 58 can be used to determine $P^*_{r\_(c+1)\_(p-1)\_O}(t)$, eqs 59 or 60 can be used to determine $P^*_{r\_(c+1)\_(p-1)\_A}(t)$, and eqs 61 or 62 can be used to determine $P^*_{(r-1)\_(c-1)\_(p-1)\_B}(t)$.

By comparing Figures 8 and 9, it is clear that not all precursors and their outgoing paths in Figure 9 are present for any configuration (block) in Figure 8. Thus, the constraints on the connective terms can be determined as follows

If $c > L$ or $c > p$, then

$$P^*_{r\_c\_p\_o}(t) = 0 \quad (64)$$

If $r > c$, then

$$P^*_{r\_c\_p\_A}(t) = 0 \quad (65)$$

If $r = 1$, $c = 0$ and $p = 0$, then

$$P^*_{r\_c\_p\_A}(t) = 1 \quad (66)$$

If $r = 0$, then

$$P^*_{r\_c\_p\_B}(t) = 0 \quad (67)$$

By following equations 39−67, it is possible to construct a system of ordinary differential equations according to a pair of chosen values for L and R to compute the time-dependent probabilities of all scenarios in the expanded structural transformation matrix. For the specific standby system described in Figure 8, expressions of the probability derivatives for all scenarios in the blocks along the first row of the first upper-triangular submatrix have already been given in Part E of the SI. To facilitate clearer illustration of the model structure, additional example expressions are provided in Part F in the SI. Notice from Figure 9 that, for a given destination block, there may be at most three incoming paths from three different precursors, respectively. Thus, the number of combinations of input patterns to a block in the expanded matrix should be 7 ($=2^3 - 1$). Since an input pattern has already been discussed previously and also in Part E in the SI, one example of each of the remaining six is presented in Part F in the SI for the sake of completeness.

6. EXPECTED LIFECYCLE LOSS

As mentioned above, all time-dependent scenario probabilities can be determined with the proposed mathematical model. For the sake of formulation conciseness, let us introduce the following notation

$$P_{r\_c\_s}(t) = \sum_{i=0}^{R} P_{r\_c\_(2i+c)\_s}(t) \quad (68)$$

It can be observed from the event trees in Figures 3−6 that scenarios 1, 2, 3, 5, and 6 result in supply-larger-than-demand losses and scenarios 4 and 7, 8, 9, 10, 11, 12, 13, 14, and 15 cause supply-smaller-than-demand losses. Thus, the total expected loss in the kth year in the operation horizon, which is denoted as $IS(k-1,k)$ in this paper, can be expressed as follows

$$IS(k-1, k) = C_a^{(k)} \sum_{s\in \mathbf{S}_a} \int_{k-1}^{k} P_{r\_c\_s}(t)dt + C_b^{(k)} \sum_{s\in \mathbf{S}_b} \int_{k-1}^{k} P_{r\_c\_s}(t)\mathrm{d}t \quad (69)$$

where $\mathbf{S}_a = \{1, 2, 3, 5, 6\}$; $\mathbf{S}_b = \{4, 7, 8, 9, 10, 11, 12, 13, 14, 15\}$; $C_a^{(k)}$ is the financial loss of a supply-larger-than-demand event occurring in the kth year of the operation horizon; and $C_a^{(k)}$ is the financial loss of a supply-smaller-than-demand event occurring in the kth year of the operation horizon. Since the length of horizon is H, the total expected lifecycle loss (denoted as IS^H) can be determined according to the following formula

$$IS^H = \sum_{k=1}^{H} IS(k-1, k) \times CF_k \quad (70)$$

where CF_k denotes a yearly factor to convert the expenditure in the kth year to present value, i.e., $CF_k = 1/r^{k-1}$ and r is the interest rate.

https://doi.org/10.1021/acs.iecr.2c04521
Ind. Eng. Chem. Res. 2023, 62, 5150−5169

7. OBJECTIVE FUNCTION

The objective function of the proposed mathematical programming model is the sum of the total expected lifecycle loss of the standby mechanism and the total capital costs of sensors, switches, and standby units,i.e.,

$$\text{obj} = IS^{H} + LCC^{sr} + LCC^{sw} + LCC^{wb} \tag{71}$$

where LCC^{sr} denotes the total expected lifecycle cost of monitoring subsystem; LCC^{sw} is the expected lifecycle cost of switches; and LCC^{wb} represents the expected lifecycle cost of warm standbys.

7.1. Total Expected Lifecycle Costs of Monitoring Subsystems. Since the spare-supported corrective maintenance policy[6] is followed to upkeep the three monitoring subsystems mentioned previously (see Part D.1 in the SI), the corresponding expenditures should include the purchase cost, the repair cost, and the replacement cost.

For the α monitoring subsystem, the purchase cost (denoted as $PCT^{sr,\alpha}$) can be expressed as

$$PCT^{sr,\alpha} = \sum_{j=1}^{J} (N_j^{sr,\alpha} + SN_j^{sr,\alpha}) \times PC_j^{sr,\alpha} \tag{72}$$

where $N_j^{sr,\alpha}$ denotes the number of online sensors in the jth channel of the α monitoring subsystem; $SN_j^{sr,\alpha}$ is the corresponding number of spares for the jth channel; $PC_j^{sr,\alpha}$ is the purchase cost of a single sensor in the jth channel of the α monitoring subsystem. On the other hand, the total expected costs of repair and replacement of the α monitoring subsystem (denoted as $RrCT^{sr,\alpha}$ and $RplCT^{sr,\alpha}$, respectively) can be determined as follows

$$RrCT^{sr,\alpha} = \sum_{j}^{J} \sum_{k}^{K} RrC_j^{sr,\alpha} \times ENRr_{j,k}^{sr,\alpha} \times CF_k \tag{73}$$

$$RplCT^{sr,\alpha} = \sum_{j}^{J} \sum_{k}^{K} RplC_j^{sr,\alpha} \times ENRpl_{j,k}^{sr,\alpha} \times CF \tag{74}$$

where $RrC_j^{sr,\alpha}$ and $RplC_j^{sr,\alpha}$ represent the costs of repairing and replacing a sensor, respectively, in the jth channel of α monitoring subsystem, and $ENRr_{j,k}^{sr,\alpha}$ and $ENRpl_{j,k}^{sr,\alpha}$ denote the corresponding expected numbers of repairs and replacements, respectively, in the jth channel of α monitoring subsystem during the kth year and they can be determined according to the computation procedures outlined in Part D.1 in the SI.

For the β monitoring subsystem, the purchase cost (denoted as $PCT^{sr,\beta}$) is

$$PCT^{sr,\beta} = \sum_{m=1}^{M} (N_m^{sr,\beta} + SN_m^{sr,\beta}) \times PC_m^{sr,\beta} \tag{75}$$

where $N_m^{sr,\beta}$ denotes the number of online sensors in the mth channel of the β monitoring subsystem; $SN_m^{sr,\beta}$ is the corresponding number of spares for the mth channel; and $PC_m^{sr,\beta}$ is the purchase cost of a single sensor in the mth channel of the β monitoring subsystem. On the other hand, the total expected costs of repair and replacement of the β monitoring subsystem (denoted as $RrCT^{sr,\beta}$ and $RplCT^{sr,\beta}$, respectively) can be expressed as

$$RrCT^{sr,\beta} = \sum_{m}^{M} \sum_{k}^{H} RrC_m^{sr,\beta} \times ENRr_{m,k}^{sr,\beta} \times CF_k \tag{76}$$

$$RplCT^{sr,\beta} = \sum_{m}^{M} \sum_{k}^{H} RplC_m^{sr,\beta} \times ENRpl_{m,k}^{sr,\beta} \times CF_k \tag{77}$$

where $RrC_m^{sr,\beta}$ and $RplC_m^{sr,\beta}$ represent the costs of repairing and replacing a sensor, respectively, in the mth channel of β monitoring subsystem, and $ENRr_{m,k}^{sr,\beta}$ and $ENRpl_{m,k}^{sr,\beta}$ denote the corresponding expected numbers of repairs and replacements in the mth channel of β monitoring subsystem during the kth year, and they can also be determined according to the computation procedures outlined in Part D.1 in the SI.

For the γ monitoring subsystem, the purchase cost (denoted as $PCT^{sr,\gamma}$) should be written differently as

$$PCT^{sr,\gamma} = \sum_{l=1}^{L} \sum_{i=1}^{I} (N_{i,l}^{sr,\gamma} + SN_{i,l}^{sr,\gamma}) \times PC_{i,l}^{sr,\gamma} \tag{78}$$

where $N_{i,l}^{sr,\gamma}$ denotes the number of online sensors in the ith channel for the ith online unit in the γ monitoring subsystem; $SN_{i,l}^{sr,\gamma}$ is the corresponding number of spares for the ith channel and the ith online unit in the γ monitoring subsystem; and $PC_{i,l}^{sr,\gamma}$ is the purchase cost of a single sensor in the ith channel for the ith online unit in the γ monitoring subsystem. On the other hand, the total expected costs of repair and replacement of the γ monitoring subsystem (denoted as $RrCT^{sr,\gamma}$ and $RplCT^{sr,\gamma}$, respectively) can be expressed as

$$RrCT^{sr,\gamma} = \sum_{l=1}^{L} \sum_{i=1}^{I} \sum_{k=1}^{H} ENRr_{i,k,l}^{sr,\gamma} \times RrC_i^{sr,\gamma} \times CF_k \tag{79}$$

$$RplCT^{sr,\gamma} = \sum_{l=1}^{L} \sum_{i=1}^{I} \sum_{k=1}^{H} ENRpl_{i,k,l}^{sr,\gamma} \times RplC_i^{sr,\gamma} \times CF_k \tag{80}$$

where $RrC_i^{sr,\gamma}$ and $RplC_i^{sr}$ represent the costs of repairing and replacing a sensor, respectively, in the ith channel of γ monitoring subsystem, and $ENRr_{i,k,l}^{sr,\gamma}$ and $ENRpl_{i,k,l}^{sr,\beta}$ denote the corresponding expected numbers of repairs and replacements in the ith channel of γ monitoring subsystem for the ith online unit during the kth year and they can also be determined according to the computation procedures outlined in Part D.1 in the SI. From the above discussion, it is clear that the total expected lifecycle cots of monitoring subsystem (denoted as LCC^{sr}) can be calculated according to the following formula

$$LCC^{sr} = \sum_{*\in\{\alpha,\beta,\gamma\}} PCT^{sr,*} \sum_{*\in\{\alpha,\beta,\gamma\}} RrCT^{sr,*} + \sum_{*\in\{\alpha,\beta,\gamma\}} RplCT^{sr,*} \tag{81}$$

7.2. Total Expected Lifecycle Costs of Switching Devices. Since the switch malfunction is considered to be a hidden failure, the preventive maintenance policy should be applied to improve its reliability. In addition, it is assumed that switches are relatively inexpensive. Therefore, if a switch is found to be broken after inspection, this failed one is discarded and a new one is immediately adopted to take its place. The corresponding purchase cost (denoted as PCT^{sw}) can be expressed as

$$PCT^{sw} = (1 + SN^{sw}) \times PC^{sw} \tag{82}$$

where SN^{sw} denotes the number of spare switches stored offline and PC^{sw} is the purchase cost of a switch. On the other hand, the total inspection cost (denoted as $InspCT^{sw}$) can be calculated according to the following formula

https://doi.org/10.1021/acs.iecr.2c04521
Ind. Eng. Chem. Res. 2023, 62, 5150−5169

$$InspCT^{sw} = \sum_{k=1}^{H} st^{sw} \times InspC^{sw} \times CF_k \tag{83}$$

where $InspCT^{sw}$ denotes the one-time inspection cost of switch and st^{sw} is the total number of inspections over the operation horizon (see Part D.2 in the SI).

Based on the above discussion, the total expected lifecycle costs of switching devices can be calculated as follows

$$LCC^{sw} = PCT^{sw} + InspCT^{sw} \tag{84}$$

7.3. Total Expected Lifecycle Costs of Warm Standbys. Let us consider an L-unit standby system. Let us also assume that there is one unit running initially and the remaining $L - 1$ units are treated as warm standbys in the beginning of operation. For each of these warm standbys, let us assume that there are also cold standbys stored offline to further enhance system reliability. Therefore, the total purchase cost of all initial standbys (denoted as PCT^{wb}) should be

$$PCT^{wb} = \sum_{l=1}^{L-1} (1 + SN_l^{wb}) \times PC^{wb} \tag{85}$$

where SN_l^{wb} is the number of cold standbys used as backups for the lth warm standby and PC^{wb} is the purchase cost of a critical unit in the standby system. On the other hand, the total expected lifecycle repair cost and inspection cost (denoted as $RrCT^{wb}$ and $InspCT^{wb}$, respectively) should be expressed as

$$RrCT^{wb} = \sum_{l=1}^{L-1} \sum_{k=1}^{H} ENRr_{k,l}^{wb} \times RrC^{wb} \times CF_k \tag{86}$$

$$InspCT^{wb} = \sum_{l=1}^{L-1} \sum_{k=1}^{H} st_{k,l}^{wb} \times InspC^{wb} \times CF_k \tag{87}$$

where RrC^{wb} and $InspC^{wb}$, respectively, represent the one-time repair and inspection costs for a single warm standby, and $ENRr_{k,l}^{wb}$ and $st_{k,l}^{wb}$, respectively, denote the expected number of repairs and the number of inspections for the lth warm standby during the kth year (see Part D.3 in the SI for further details).

Based on the above discussion, the total expected lifecycle cost of a warm standby can be determined as follows

$$LCC^{wb} = PCT^{wb} + RrCT^{wb} + InspCT^{wb} \tag{88}$$

7.4. Mathematical Programming Model. Finally, it should be noted that the total expected lifecycle expenditure defined previously in eq 71 was used as the objective function of the integer programming model in each of the case studies presented in this paper. The model constraints are described in all aforementioned formulations (except the objection function mentioned above) and those in Parts A, C, D, E, and F of the SI. Finally, all binary and ternary numbers in the constraints are considered to be the decision variables in this model.

8. CASE STUDIES

The feasibility and effectiveness of the proposed optimization strategy are demonstrated in the case studies in this section. Although, as mentioned before, the proposed model is suitable for a wide variety of applications, let us consider the simple four-unit pump system in Figure 10 for the sake of illustration clarity. As depicted in this figure, pump #1 is running initially and the others are the warm standbys. Let us also assume that

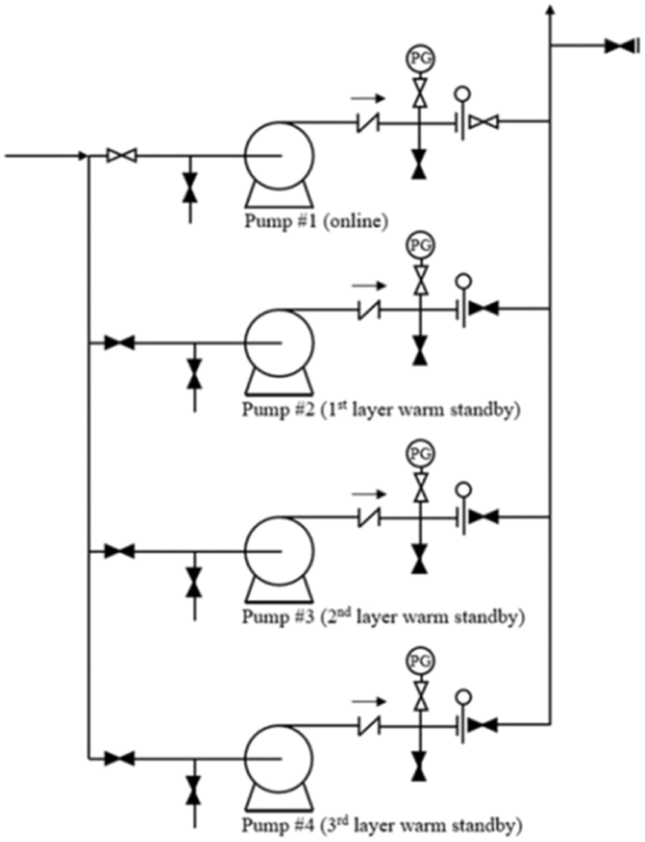

Figure 10. Four-unit pump system.

- the downstream demand can be determined with the α monitoring subsystem via flow measurement.
- the total upstream system output is evaluated with the β monitoring subsystem according to flow and pressure measurements.
- the failure of every online pump is detected by γ monitoring subsystem through measurements of motor speed and discharge pressure.

The specifications of sensors, switches, and warm standbys are taken from Cadwallader[30] and Mannan,[31] and they are listed in Tables 1−3, respectively. Note that the failure rate of an online unit is chosen to be twice as large as that of each warm standby (i.e., $\lambda_f = 0.61$ year^{-1}).

Table 1. Design Specifications of Sensors

	flow rate	motor speed	pressure
failure rate (1/year)	2.4	1.3	1.41
repair rate (1/year)	3.0	2.7	2.7
replacement rate (1/year)	365	365	365
purchase cost (USD)	90	250	350
repair cost (USD)	15	20	25
replacement cost (USD)	5	10	15

Table 2. Design Specifications of Switching Devices

failure rate (1/year)	0.22
purchase cost (USD)	100
inspection cost (USD)	20
probability of FS failure	0.2

https://doi.org/10.1021/acs.iecr.2c04521
Ind. Eng. Chem. Res. 2023, 62, 5150−5169

Table 3. Design Specifications of Warm Standbys

failure rate (1/year)	0.61
repair rate (1/year)	2.5
purchase cost (USD)	2500
repair cost (USD)	100
inspection cost (USD)	50
probability of FS failure	0.2

It is assumed that the entire operational horizon (lifecycle) is 2 years, i.e., $H = 2$, while the interest rate is 3%. The maximum numbers of online sensors and spare sensors are both fixed at 2 in each channel, while each warm standby in every layer is equipped with one cold standby. Furthermore, the maximum lengths of inspection intervals for switch and warm standbys are both set to be 4 months.

To attain the desired qualities of conciseness, portability, and maintainability for easy implementation, there are strong incentives to develop a generic and modularized code on the basis of an evolutionary algorithm. A general-purpose genetic algorithm (GA) code was developed by Lepar et al.[32] to ensure modularity and conciseness and the same approach has also been chosen in the present study for the reasons mentioned above. The optimization runs were carried out according to the genetic algorithm (GA) in Matlab R2020a environment on an Intel Core i7-9700 3.0 GHz PC. This Matlab code can also be developed for any other applications on the basis of the generalized model presented in this paper and a user-specified maximum allowable layer number. In the case studies presented here, the maximum allowable number of protection layers is chosen to be four, i.e., $L \leq 4$. In applying GA for the case studies, the maximum number of generations was set to be 50, the number of individuals in each generation was set to be 180, and the crossover and mutation probability were chosen to be 0.80 and 0.03, respectively. The computation time of an optimization run varies roughly between 5000 and 18,000 s.

Although various combinations of the financial losses of supply-larger-than-demand event and supply-smaller-than-demand event have been evaluated, only the optimization results for $C_a^{(k)} = 0$ USD and $C_b^{(k)} = 10^6$ USD ($k = 1, 2$) are summarized in Tables 4 and 5, and those for $C_a^{(k)} = 10^5$ USD and $C_b^{(k)} = 10^5$ USD ($k = 1, 2$) are given in Table 6. For the sake of brevity, the corresponding convergence behaviors in the optimization runs and the resulting optimal system configurations are shown in Part G of the Supporting Information for Publication. Notice also that, although there are no budget constraints imposed on the cases in Tables 5 and 6, the upper limit of the capital investment for every case in Table 4 was arbitrarily chosen to be 12,000 USD simply for the purpose of testing the effects of impose budget constraint(s). Finally,

Table 4. Optimization Results of Three Test Cases with Budget Constraints ($C_a = 0$; $C_b = 10^6$)

case no.	#1	#2	#3
budget limit (USD)	12,000	12,000	12,000
$\lambda_{\pm}$ (year^{-1})	0.5	2.0	5.0
objective function (USD)	693,540	674,799	659,267
total expected lifecycle loss (USD)	683,558	664,987	649,343
total purchase cost (USD)	7890	7710	7800
total expected maintenance cost (USD)	2092	2102	2124
computation time (minutes)	92	101	106

Table 5. Optimization Results of the Same Cases without Budget Constraints ($C_a = 0$; $C_b = 10^6$)

case no.	#4	#5	#6
budget limit (USD)			
$\lambda_{\pm}$ (year^{-1})	0.5	2.0	5.0
objective function (USD)	308,785	357,208	368,992
total expected lifecycle loss (USD)	283,578	332,249	345,161
total purchase cost (USD)	20,370	20,120	19,600
total expected maintenance cost (USD)	4838	4839	4230
computation time (minutes)	164	188	299

Table 6. Optimization Results of Another Three Cases with Identical Cost Constants without Budget Constraints ($C_a = 10^5$; $C_b = 10^5$)

case no.	#7	#8	#9
budget limit (USD)			
$\lambda_{\pm}$ (year^{-1})	0.5	2.0	5.0
objective function (USD)	73,405	69,653	66,280
total expected lifecycle loss (USD)	49,992	47,123	43,853
total purchase cost (USD)	19,250	19,160	19,160
total expected maintenance cost (USD)	4163	3369	3267
computation time (minutes)	138	145	135

Figures 11−19 show the expected losses of each and every scenario in the optimum solutions of Cases #1−#9 (see Tables 4−6), respectively.

By comparing Tables 4 and 5, it can be clearly observed that the objective values listed in the former table are much higher than those in the latter. This is due to the additional budget limits imposed on the three cases in Table 4. Owing to this financial constraint, only one warm standby is allowed to be installed in each case of Table 4 and the undesirable aspect of lacking enough protection is reflected in the corresponding total expected lifecycle losses. On the other hand, notice from Table 4 that the expected loss gradually decreases as $\lambda_{\pm}$ increases from Case #1 to Case #3. Notice also that only a two-by-two structural transformation matrix is needed to characterize the transition processes in each of the above three cases. It can be observed from Figures 1−3 that larger expected losses generally result from scenarios that take place in configurations associated with matrix entries (1,2), i.e., $r = 1$ and $c = 2$, and also (2,2), i.e., $r = 2$ and $c = 2$, since the corresponding systems are without the protection of any warm standby. It should also be noted that, among the optimization results obtained for all possible scenarios in Figures 1−3, the expected losses of scenarios 14 and 15 are dominant and their trends are dependent upon the ratio λ_+/λ_f. If the value of λ_+/λ_f is large, the probability of load change in entry (1,2) is relatively high. Otherwise, the probability of online unit failure in entry (2,2) should be larger. Finally, let's examine the event trees for Mode I^0 (Figure 4) and Mode II^0 (Figure 6). Notice that these two trees are located in entry (2,2) and entry (1,2), respectively, in the structural transformation matrix. Since the optimization results in Table 4 were obtained by setting $C_a = 0$ and $C_b = 10^6$, only the supply-smaller-than-demand scenarios yield losses. All valid scenarios in the Mode I^0 tree, i.e., scenarios 14 and 15, result in such losses, while half of the scenarios in Mode II^0 tree do not incur penalties, i.e., scenarios 1, 2 and 3, since they are classified in this study as the supply-larger-than-demand events. This feature also contributes significantly to the aforementioned effects produced by varying λ_+/λ_f.

https://doi.org/10.1021/acs.iecr.2c04521
Ind. Eng. Chem. Res. 2023, 62, 5150−5169

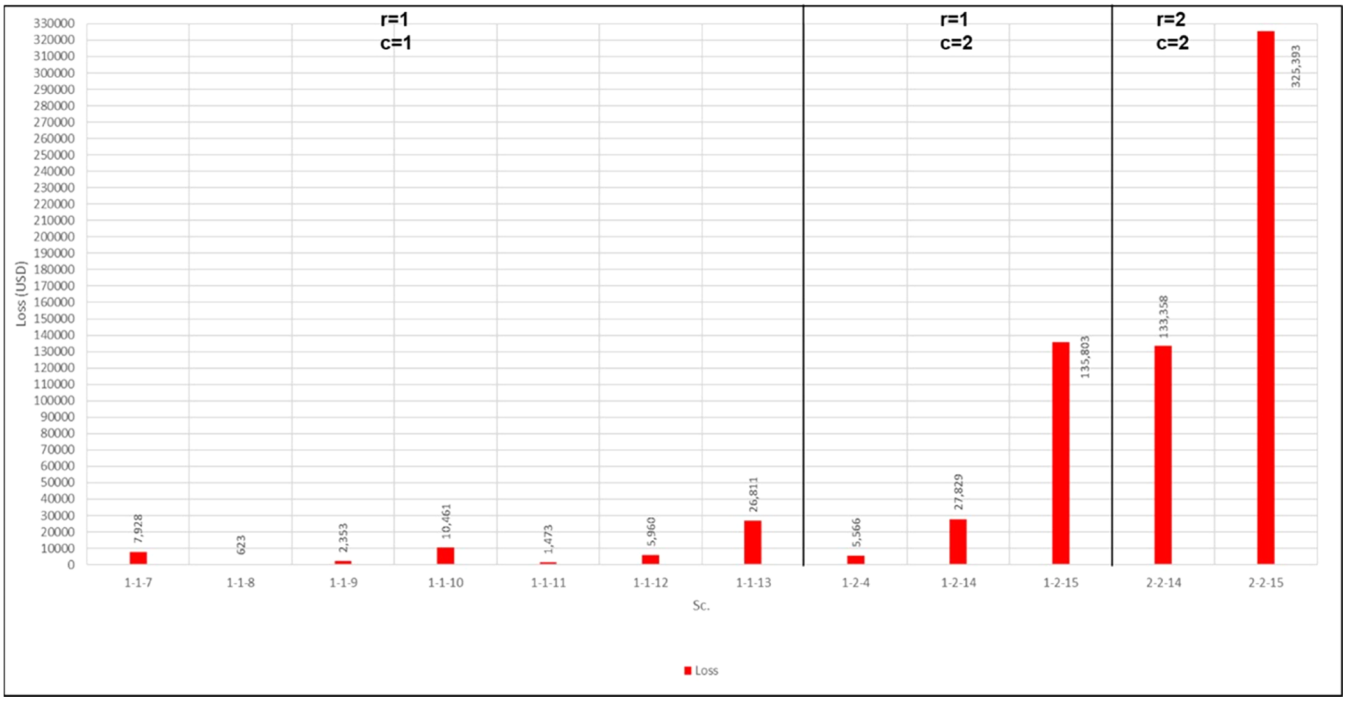

Figure 11. Expected losses of all scenarios in Case #1.

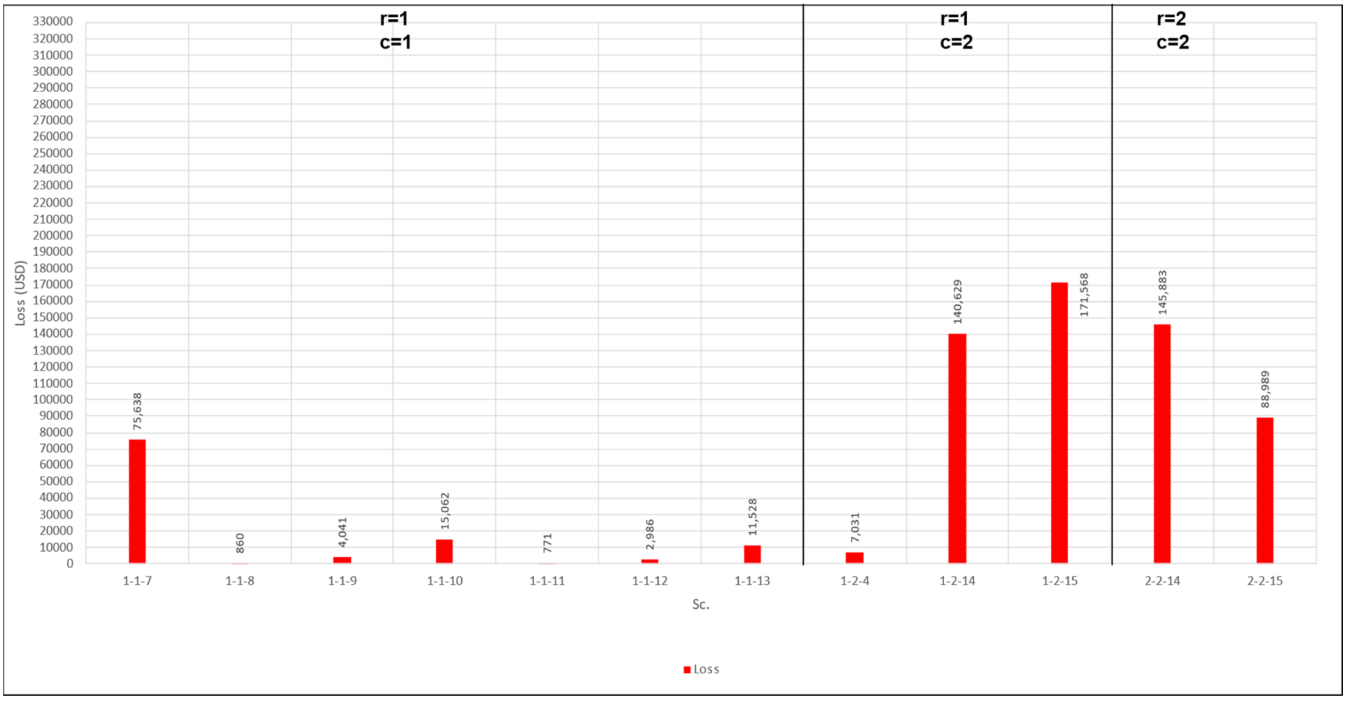

Figure 12. Expected losses of all scenarios in Case #2.

As mentioned above, the objective values of cases with financial constraints (Table 4) tend to be much larger than those without limits (Table 5). Notice from the latter table that the expected loss slowly increases as $\lambda_{\pm}$ (or λ_{+}/λ_{f}) increases from Case #4 to Case #6, and this trend is different from that exhibited in Case #1−Case #3. Notice also that a four-by-four structural transformation matrix is needed to characterize the transition processes in each case of Table 5. It can be observed from Figures 4−6 that larger expected losses generally result from the scenarios that take place in configurations associated with matrix entries (1,4), (2,4), (3,4), and (4,4) because the corresponding systems are without functional warm standby. On the other hand, the sum of expected losses in entries of row 1 or 2 in structural transformation matrix increases as $\lambda_{\pm}$ increases, but the opposite trend can be observed from row 3 or 4. Furthermore, the total number of nonempty entries in rows 1 and 2 is larger than that in rows 3 and 4. In summary, the aforementioned observations may cause the combined effects of the overall expected loss gradually increasing with $\lambda_{\pm}$ from Case #4 to Case #6. Finally, there are still a few additional features

https://doi.org/10.1021/acs.iecr.2c04521
Ind. Eng. Chem. Res. 2023, 62, 5150−5169

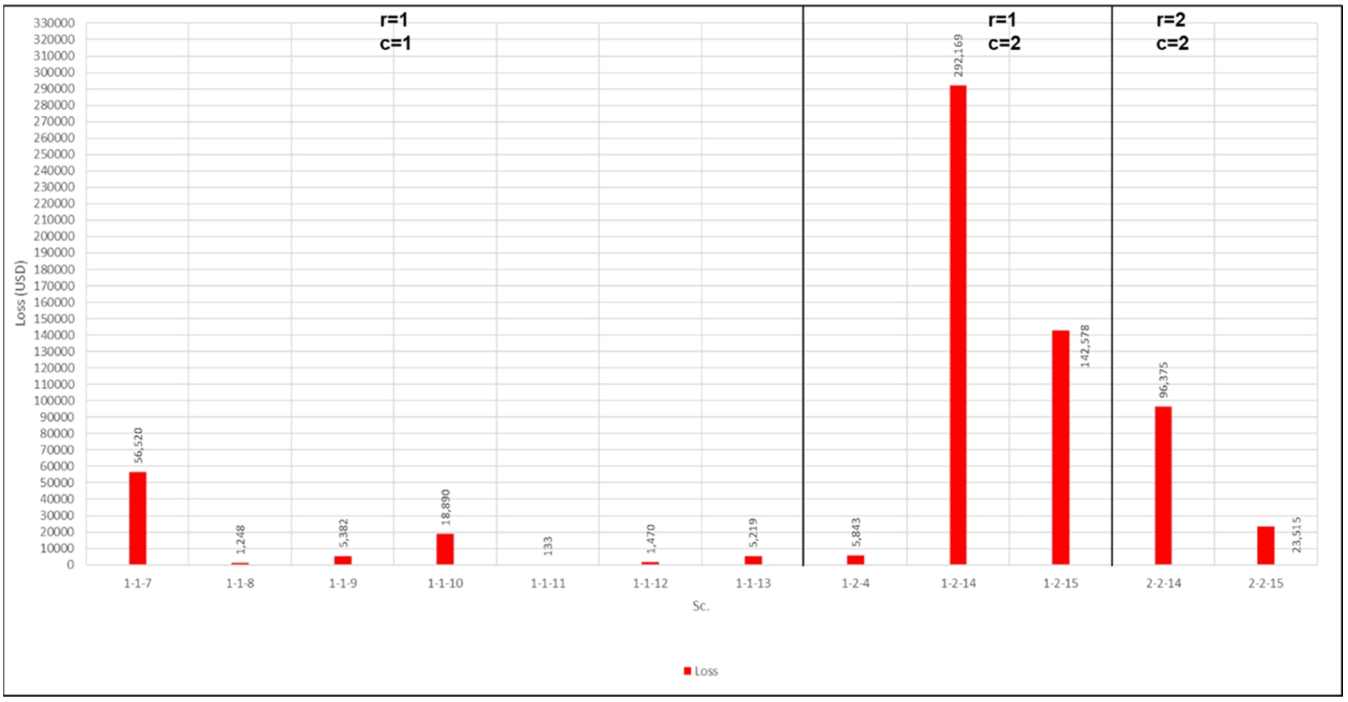

Figure 13. Expected losses of all scenarios in Case #3.

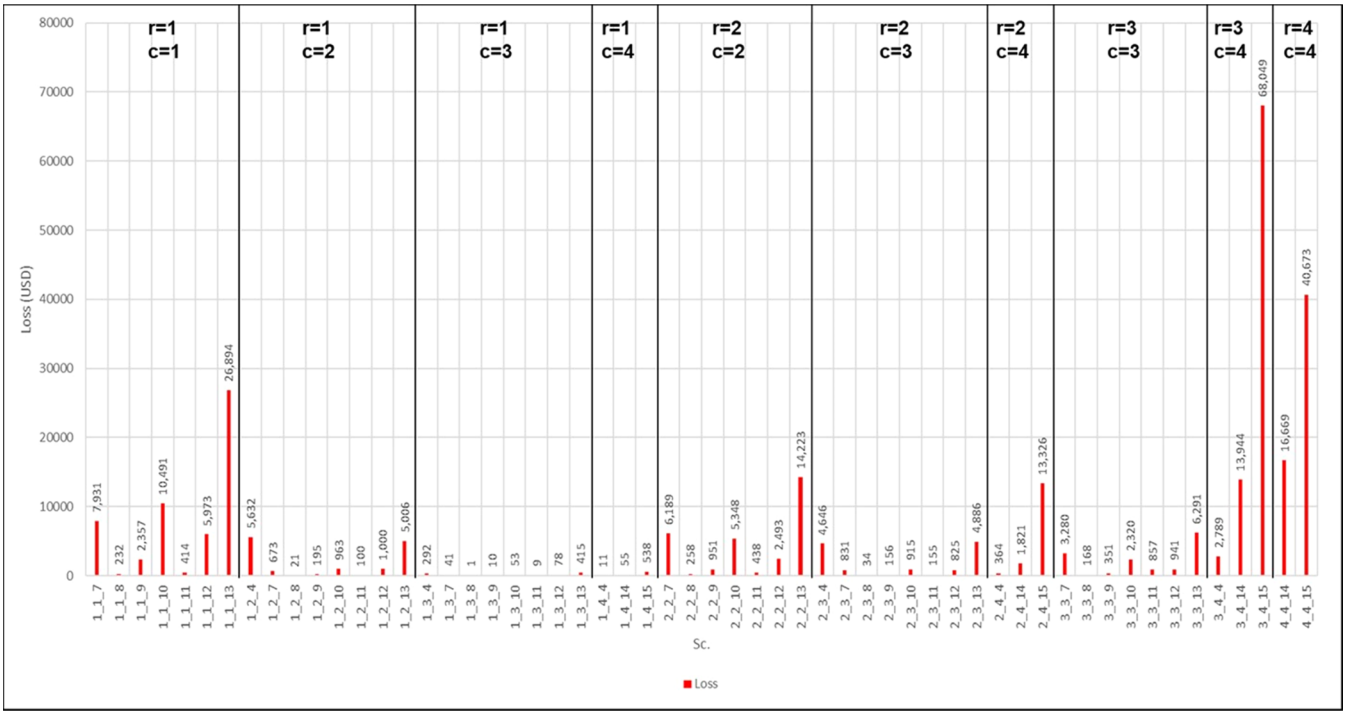

Figure 14. Expected losses of all scenarios in Case #4.

embedded in Figures 4−6 which are worth mentioning. Notice first that scenarios 7, 8, and 11 in entries (1,1), (1,2), (1,3), (2,2), (2,3), and (3,3) (which can also be found in Figures 3 and 5) result in FD failures of the measurement channels. In Case #4 and Case #5, scenario 7 causes the highest loss among the three. This is due to the fact that α monitoring system possesses only a single measurement channel while each of the other two has two channels (see Appendix G in the SI). Also, notice that the expected loss resulting from every scenario 8 in Case #6 is much larger than the corresponding scenario in Case #4 or Case #5. This is because a 2-out-of-2 voting gate is adopted in each β channel of Case #6 while a 1-out-of-1 gate and a 1-out-of-2 gate are used in case #4 and Case #5, respectively.

The optimization results obtained in the last three cases (Case #7−Case #9) are different from those in Tables 4 and 5 in the sense that the costs of the supply-larger-than-demand and the supply-smaller-than-demand events are equal, i.e., $C_a = C_b = 10^5$. Figures 7−9 show the corresponding expected losses of each and

https://doi.org/10.1021/acs.iecr.2c04521
Ind. Eng. Chem. Res. 2023, 62, 5150−5169

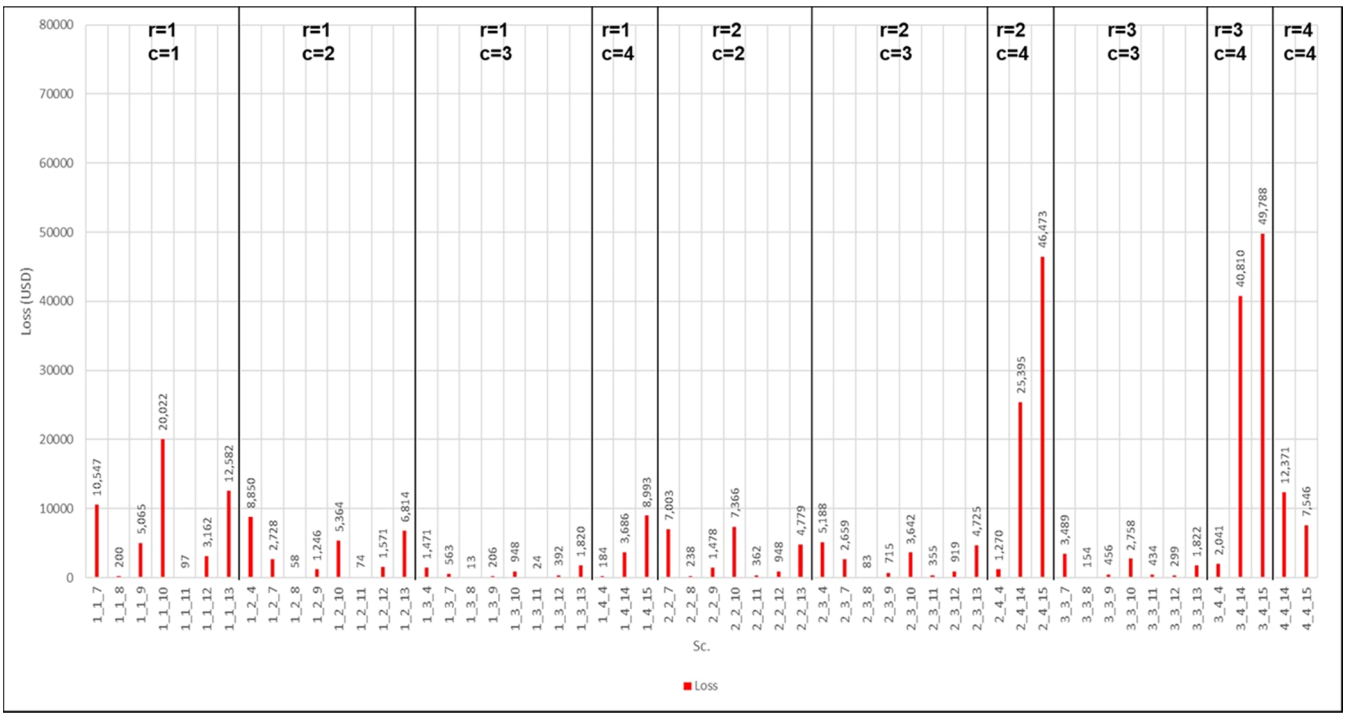

Figure 15. Expected losses of all scenarios in Case #5.

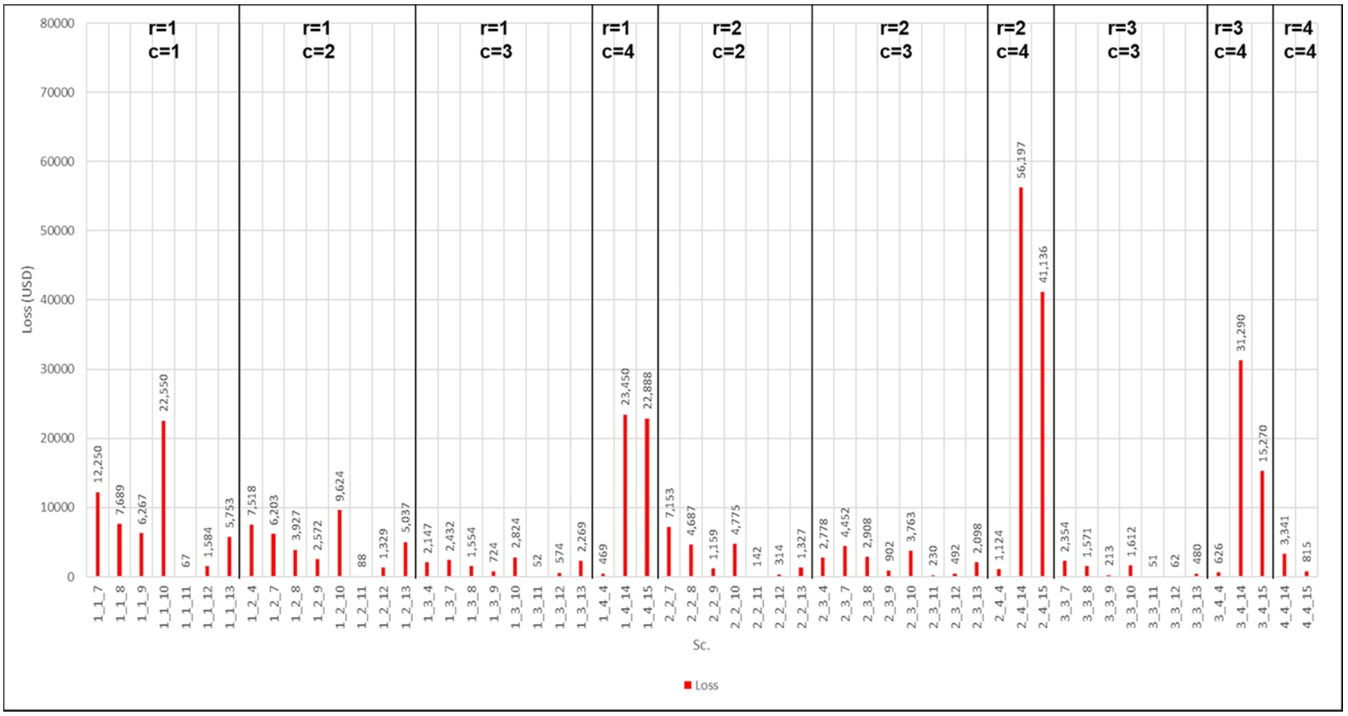

Figure 16. Expected losses of all scenarios in Case #6.

every scenario in optimum solutions of Cases #7−#9 in Table 6, respectively. In these figures, the supply-smaller-than-demand scenarios are marked in red, while the supply-larger-than-demand scenarios blue. It can be observed from Table 6 that the total lifecycle expected loss decreases as $\lambda_{\pm}$ (or λ_{+}/λ_{f}) increases from Case #7 to Case #9. It can also be observed from Figures 7−9 that larger supply-smaller-than-demand losses generally occur in configurations associated with matrix entries (1,4), (2,4), (3,4), and (4,4), e.g., scenarios 14 and 15, again because the corresponding systems are without warm standby. These expected losses in entries (1,4) and (2,4) increase as $\lambda_{\pm}$ increases, but the opposite trends take place in entries (3,4) and (4,4). On the other hand, the larger supply-larger-than-demand losses can usually be found in Mode-I and Mode-II configurations (see scenarios 5 and 6 in Figures 7 −9 and their descriptions in Part B in the SI). Notice from Figures 7−9 that the expected losses of scenarios 5 and 6 in Mode-I configurations, which are located in entries (1,1), (2,2), and

https://doi.org/10.1021/acs.iecr.2c04521
Ind. Eng. Chem. Res. 2023, 62, 5150−5169

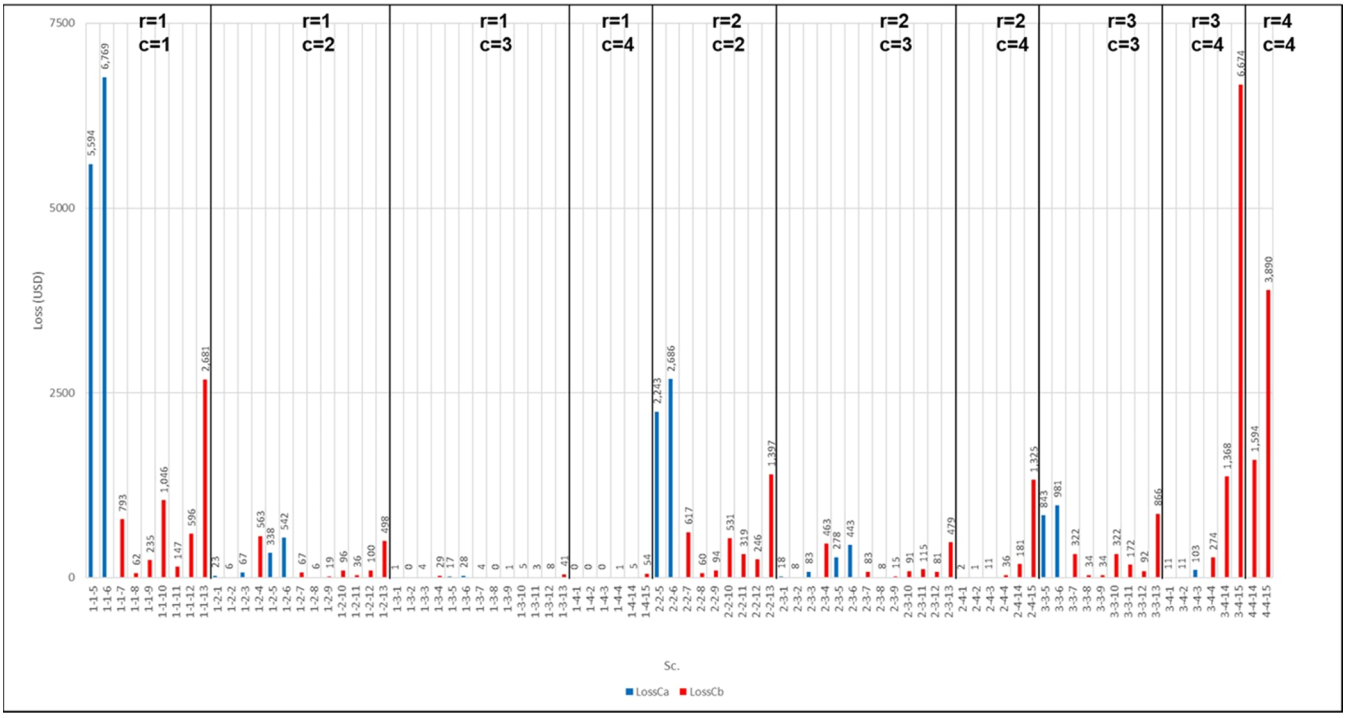

Figure 17. Expected losses of all scenarios in Case #7.

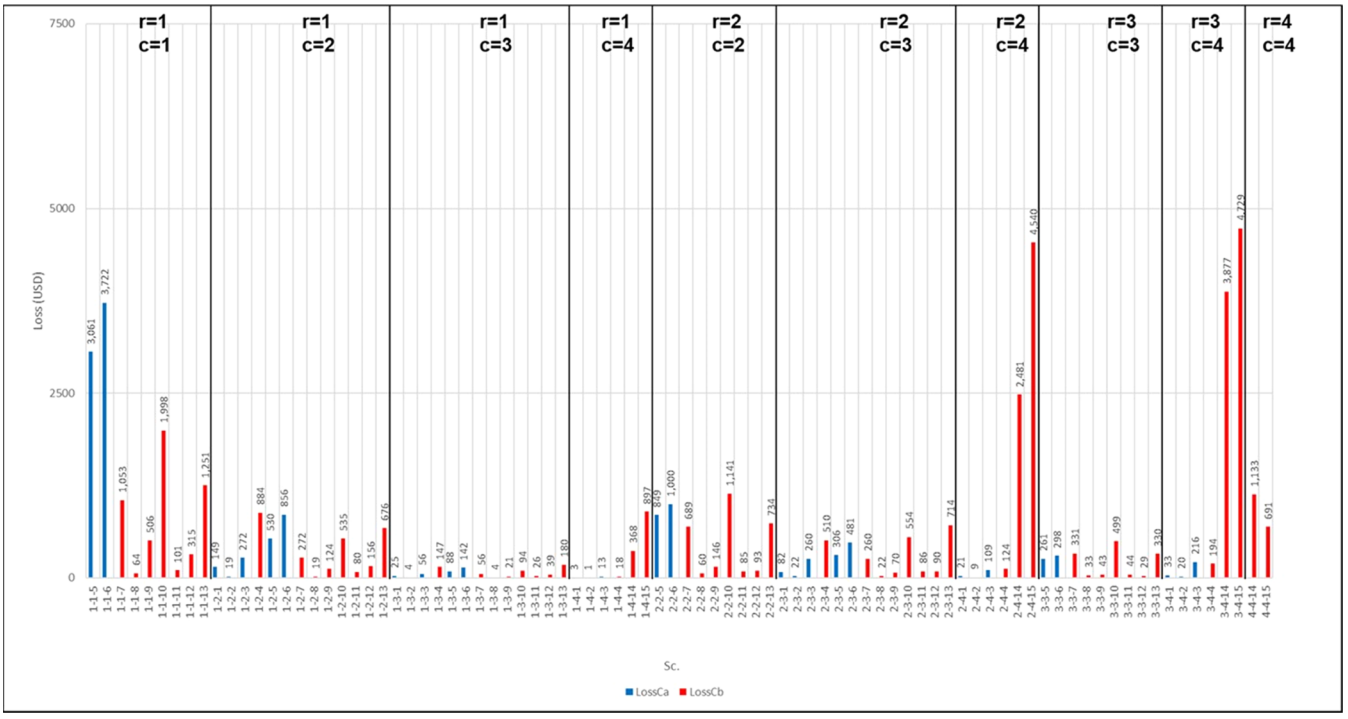

Figure 18. Expected losses of all scenarios in Case #8.

(3,3), decrease as the value of $\lambda_{\pm}$ increases. This is due to the fact that, as the ratio λ_{+}/λ_{f} increases, the chances of FS failures in scenarios 5 and 6 become lower and the probability of system visiting the above-mentioned Mode-I entries also reduces. On the other hand, the expected losses of scenarios 5 and 6 in Mode-II configurations, which are located in entries (1,2), (1,3), and (2,3), vary insignificantly as the value of $\lambda_{\pm}$ increases. This is due to the fact that, as the ratio λ_{+}/λ_{f} increases, the chances of FS failures in scenarios 5 and 6 become lower but the probability of system visiting the above-mentioned Mode-II entries increases. Based on the above discussions, the combined effect on the total lifecycle expected loss in Table 6 can be clearly observed, i.e., this loss gradually decreases as $\lambda_{\pm}$ (or λ_{+}/λ_{f}) increases from Case #7 to Case #9.

9. CONCLUSIONS

As mentioned previously in the Introduction section, not only the critical unit in a continuous process may fail unexpectedly,

https://doi.org/10.1021/acs.iecr.2c04521
Ind. Eng. Chem. Res. 2023, 62, 5150−5169

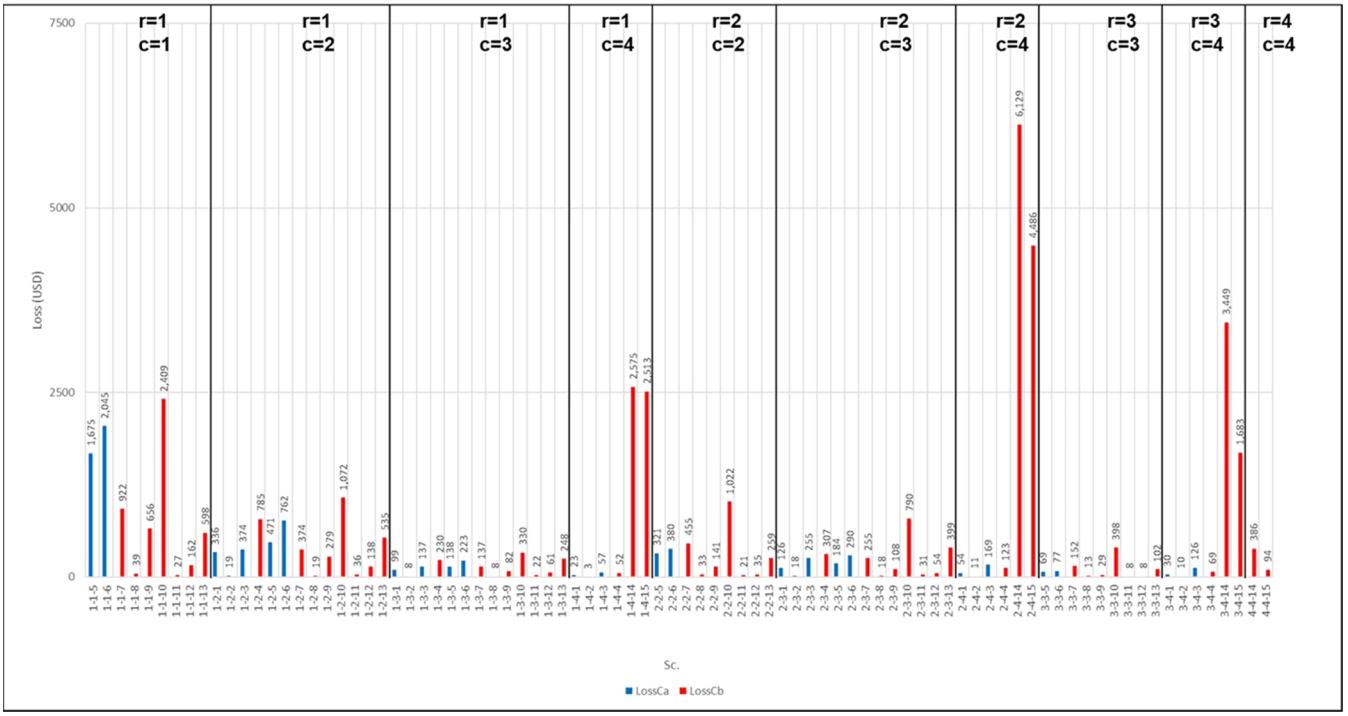

Figure 19. Expected losses of all scenarios in Case #9.

but also its load can vary from time to time. It is therefore necessary to install standbys to maintain uninterrupted production and at the same time to fully satisfy the changing demand. The availability (or reliability) of standby mechanism has been analyzed in this study rigorously on the basis of the corresponding event trees. A comprehensive mathematical programming model has also been developed accordingly to synthesize the optimal designs and maintenance policies for any process that needs the protection of standbys. The feasibility and effectiveness of the proposed approach are demonstrated in this paper with extensive case studies. Note that the quantitative optimization results in all case studies have already been partially presented and discussed in Section 8. Detailed numerical values of the optimal specifications obtained in case studies can be found in Part G of the SI. From these results, one can determine the best design specifications of the standby systems under consideration, which include: (1) the respective numbers of warm and cold standbys, (2) the total numbers of both online and spare sensors in each measurement channel and the corresponding voting-gate logic, and (3) the inspection interval of online switch and the number of its spares.

■ ASSOCIATED CONTENT

Supporting Information

The Supporting Information is available free of charge at https://pubs.acs.org/doi/10.1021/acs.iecr.2c04521.

(A) Superstructures; (B) detailed descriptions of all scenarios in the event trees; (C) probability expressions of component failures; (D) maintenance policies; (E) probabilities of scenarios embedded in the first row of the first upper-triangular submatrix and their derivatives; (F) examples of various connection routes in the expanded structural transformation matrix; and (G) optimal standby configurations obtained in case studies and the corresponding convergence behaviors of GA-based optimization runs (PDF)

■ AUTHOR INFORMATION

Corresponding Author

Chuei-Tin Chang − *Department of Chemical Engineering, National Cheng Kung University, Tainan 70701, Taiwan, ROC;* orcid.org/0000-0002-4143-1873; Email: ctchang@mail.ncku.edu.tw

Author

Cheng-I Tu − *Department of Chemical Engineering, National Cheng Kung University, Tainan 70701, Taiwan, ROC*

Complete contact information is available at: https://pubs.acs.org/10.1021/acs.iecr.2c04521

Notes

The authors declare no competing financial interest.

■ ACKNOWLEDGMENTS

This work was supported by the Ministry of Science and Technology of the Taiwan government under Grant 108-2221-E-006-149.

■ REFERENCES

(1) Zhang, T.; Xie, M.; Horigome, M. Availability and Reliability of k-out-of-(M+ N): G Warm Standby Systems. *Reliab. Eng. Syst. Saf.* **2006**, *91*, 381−387.

(2) Chan, S.-Z.; Liu, H.-Y.; Luo, Y.-K.; Chang, C.-T. Optimization of Multilayer Standby Mechanisms in Continuous Chemical Processes. *Ind. Eng. Chem. Res.* **2020**, *59*, 2049−2059.

(3) Chan, S.-Z.; Chang, C.-T. Optimization of Multilayer Standby Mechanisms in Continuous Processes under Varying Loads. *Chem. Eng. Res. Des.* **2021**, *166*, 86−96.

(4) Kuo, W.; Zuo, M. J. *Optimal Reliability Modeling: Principles and Applications*; John Wiley & Sons: Hoboken, New Jersey, 2003.

(5) Liang, K.-H.; Chang, C.-T. A Simultaneous Optimization Approach to Generate Design Specifications and Maintenance Policies for the Multilayer Protective Systems in Chemical Processes. *Ind. Eng. Chem. Res.* **2008**, *47*, 5543−5555.
(6) Liao, Y.-C.; Chang, C.-T. Design and Maintenance of Multi-channel Protective Systems. *Ind. Eng. Chem. Res.* **2010**, *49*, 11421−11433.
(7) Vaurio, J. Availability and Cost Functions for Periodically Inspected Preventively Maintained Units. *Reliab. Eng. Syst. Saf.* **1999**, *63*, 133−140.
(8) Badía, F. G.; Berrade, M. D.; Campos, C. A. Optimization of Inspection Intervals Based on Cost. *J. Appl. Probab.* **2001**, *38*, 872−881.
(9) Duarte, J. A. C.; Craveiro, J. C. T. A.; Trigo, T. P. Optimization of the Preventive Maintenance Plan of a Series Components System. *Int. J. Press. Vessels Pip.* **2006**, *83*, 244−248.
(10) Nakagawa, T.; Osaki, S. Stochastic Behaviour of a Two-Unit Standby Redundant System. *Inf. Syst. Oper. Res.* **1974**, *12*, 66−70.
(11) Nakagawa, T. A 2-Unit Repairable Redundant System with Switching Failure. *IEEE Trans. Reliab.* **1977**, *26*, 128−130.
(12) Pan, J.-N. Reliability Prediction of Imperfect Switching Systems Subject to Weibull Failures. *Comput. Ind. Eng.* **1998**, *34*, 481−492.
(13) Raje, D.; Olaniya, R.; Wakhare, P.; Deshpande, A. W. Availability Assessment of a Two-Unit Standby Pumping System. *Reliab. Eng. Syst. Saf.* **2000**, *68*, 269−274.
(14) Yun, W. Y.; Cha, J. H. Optimal Design of a General Warm Standby System. *Reliab. Eng. Syst. Saf.* **2010**, *95*, 880−886.
(15) Zhong, C.; Jin, H. A Novel Optimal Preventive Maintenance Policy for a Cold Standby System Based on Semi-Markov Theory. *Eur. J. Oper. Res.* **2014**, *232*, 405−411.
(16) Hellmich, M.; Berg, H.-P. Markov Analysis of Redundant Standby Safety Systems under Periodic Surveillance Testing. *Reliab. Eng. Syst. Saf.* **2015**, *133*, 48−58.
(17) Levitin, G.; Xing, L.; Dai, Y. Nonhomogeneous 1-Out-of-N Warm Standby Systems with Random Replacement Times. *IEEE Trans. Reliab.* **2015**, *64*, 819−828.
(18) Kayedpour, F.; Amiri, M.; Rafizadeh, M.; Shahryari Nia, A. Multi-Objective Redundancy Allocation Problem for a System with Repairable Components Considering Instantaneous Availability and Strategy Selection. *Reliab. Eng. Syst. Saf.* **2017**, *160*, 11−20.
(19) Zhu, P.; Lv, R.; Guo, Y.; Si, S. Optimal Design of Redundant Structures by Incorporating Various Costs. *IEEE Trans. Reliab.* **2018**, *67*, 1084−1095.
(20) Zhai, Q.; Peng, R.; Xing, L.; Yang, J. Binary Decision Diagram-Based Reliability Evaluation of k-out-of-(n+ k) Warm Standby Systems Subject to Fault-Level Coverage. *Proc. Inst. Mech. Eng. O: J. Risk Reliab.* **2013**, *227*, 540−548.
(21) Jia, H.; Ding, Y.; Peng, R.; Song, Y. Reliability Evaluation for Demand-Based Warm Standby Systems Considering Degradation Process. *IEEE Trans. Reliab.* **2017**, *66*, 795−805.
(22) Naithani, A.; Parashar, B.; Bhatia, P.; Taneja, G. Probabilistic Analysis of a 3-Unit Induced Draft Fan System with one Warm Standby with Priority to Repair of the Unit in Working State. *Int. J. Syst. Assur. Eng. Manag.* **2017**, *8*, 1383−1391.
(23) Amari, S. V.; Xing, L.; Shrestha, A.; Akers, J.; Trivedi, K. S. Performability Analysis of Multistate Computing Systems using Multivalued Decision Diagrams. *IEEE Trans. Comput.* **2010**, *59*, 1419−1433.
(24) Jia, H.; Liu, D.; Li, Y.; Ding, Y.; Liu, M.; Peng, R. Reliability Evaluation of Power Systems with Multi-State Warm Standby and Multi-State Performance Sharing Mechanism. *Reliab. Eng. Syst. Saf.* **2020**, *204*, No. 107139.
(25) Ruan, S.-J.; Lin, Y.-H. Reliability analysis and state transfer scheduling optimization of degrading load-sharing system equipped with warm standby components. *Proc. Inst. Mech. Eng. O: J. Risk Reliab.* **2021**, *235*, 1166−1179.
(26) Rausand, M.; Hoyland, A. *System Reliability Theory: Models, Statistical Methods, and Applications*, 2nd ed.; John Wiley & Sons: Hoboken, 2004.
(27) Pantula, P. D.; Mitra, K. A Data-Driven Approach Towards Finding Closer Estimates of Optimal Solutions under Uncertainty for an Energy Efficient Steel Casting Process. *Energy* **2019**, *189*, No. 116253.
(28) Pantula, P. D.; Mitra, K. Towards Efficient Robust Optimization using Data based Optimal Segmentation of Uncertain Space. *Reliab. Eng. Syst. Saf.* **2020**, *197*, No. 106821.
(29) Liptak, B. G. *Optimization of Unit Operations*; CRC Press: Boca Raton, Florida, 1987.
(30) Cadwallader, L. C. *Reliability Estimates for Selected Sensors in Fusion Applications*; Lockheed Idaho Technologies Co: Idaho Falls, USA, 1996.
(31) Mannan, S. *Lee's Loss Prevention in the Process Industries: Hazard Identification, Assessment and Control*, 4th ed.; Butterworth-Heinemann: Oxford, United Kingdom, 2012.
(32) Lepar, Y. Y.; Wang, Y.-C.; Chang, C.-T. Automatic Generation of Interlock Designs Using Genetic Algorithms. *Comput. Chem. Eng.* **2017**, *101*, 167−192.

https://doi.org/10.1021/acs.iecr.2c04521
Ind. Eng. Chem. Res. 2023, 62, 5150−5169